Derivation of Level 2 Products:
Terrestrial and Aquatic Surface Reflectances

Bo-Cai Gao

Remote Sensing Division,
Naval Research Laboratory, Washington, DC USA

OUTLINE

- Atmospheric corrections over land
- Atmospheric corrections over water
- Discussions and summary
- BACKUP slides: Cirrus corrections for improved retrieval of ocean, land, and atmospheric data products

Part I: Land Version of the Atmospheric Correction Algorithm

The Concept of Imaging Spectrometry

The concept of imaging spectrometry was originated at NASA JPL in the mid-1980s. Geologists hoped to have images and spectra for direct identifications of minerals from remote sensing data.

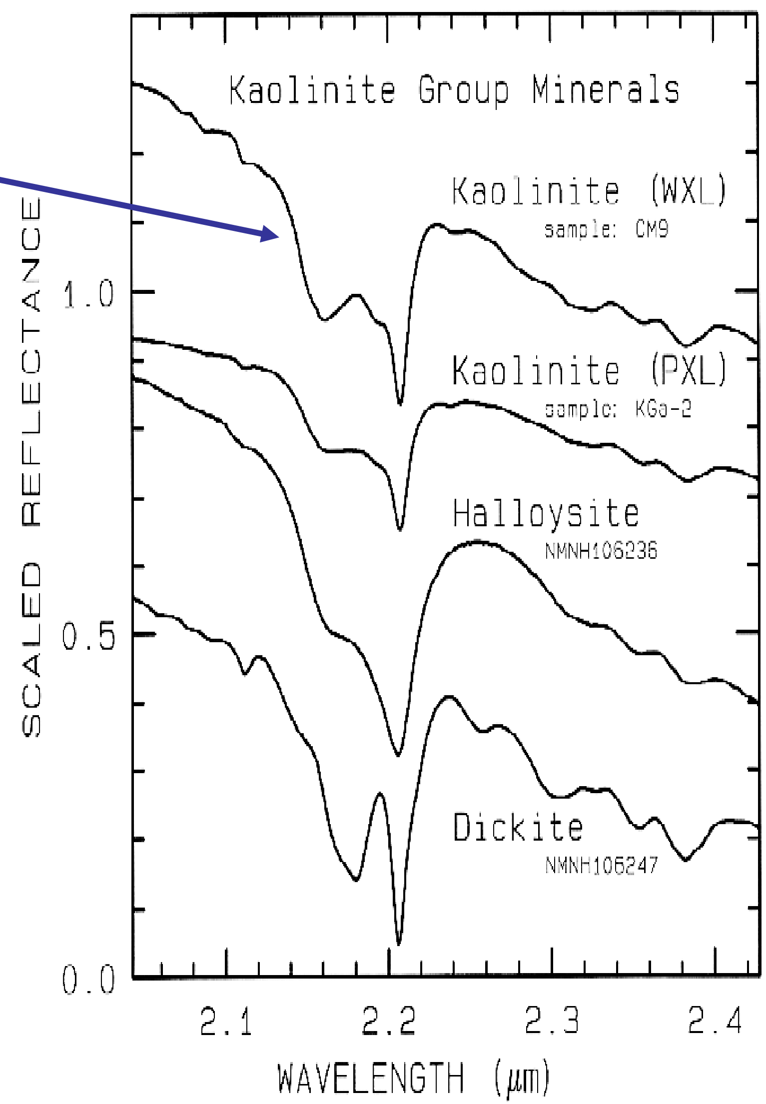

Dr. Alex. Geotz is the father of imaging spectrometry. He also envisioned the need of a model-based atmospheric correction algorithm in the late 1980s.

I worked with Dr. Goetz at U. of Colorado from 1988 to 1992 for the NASA EOS HIRIS Project to develop the 1st hyperspectral atmospheric correction algorithm - ATREM. The source code of ATREM was publicly released through U. of Colorado to more than 300 researchers worldwide.

Atmospheric Correction Over Land

An AVIRIS Spectrum

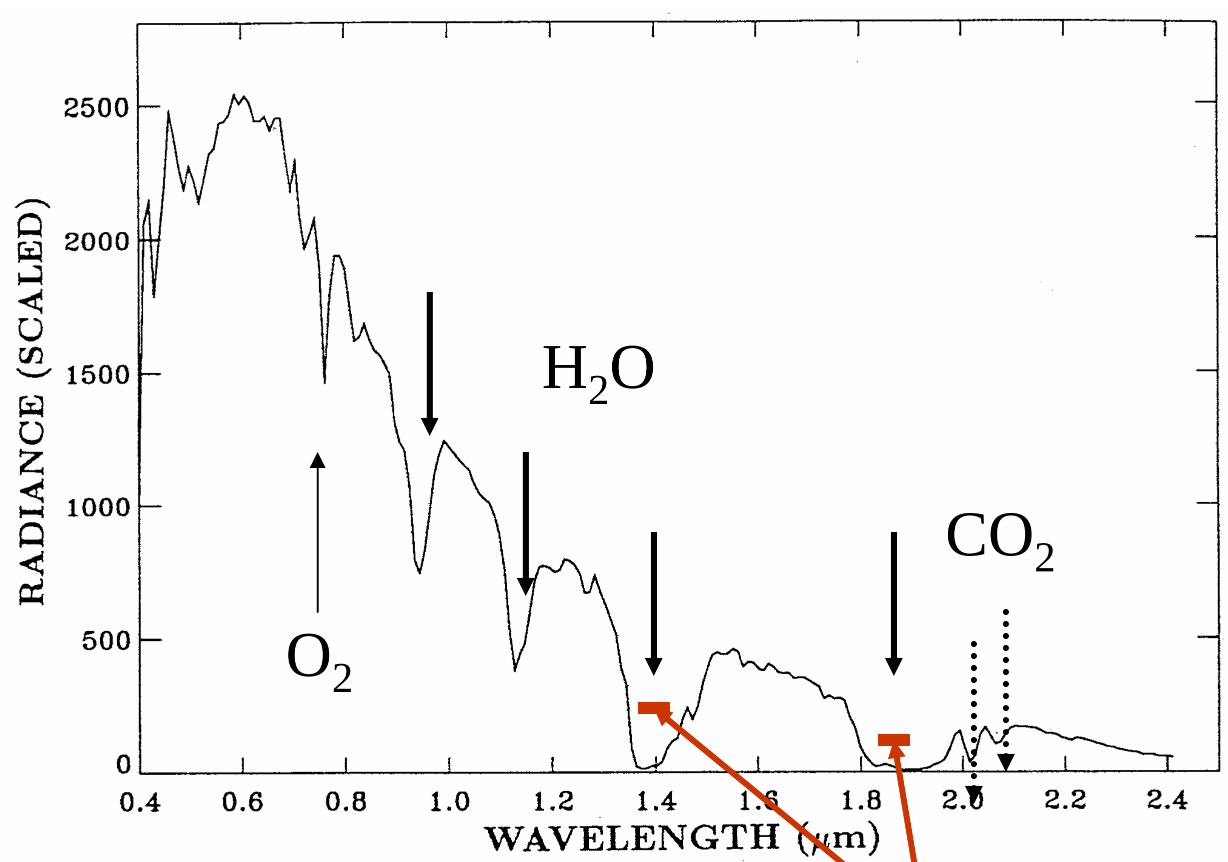

The AVIRIS spectrum is affected by atmospheric absorption and scattering effects. In order to obtain the surface reflectance spectrum, the atmospheric effects need to be removed.

Strong water vapor bands are located near 1.38 and 1.88 micron. No signals are detected under clear sky conditions.

Aerosol Scattering Effects

True Color Image
(R: 0.66, G: 0.55, B: 0.47 μm)

False Color Image
(R: 2.13, G: 1.24, B: 1.64 μm)

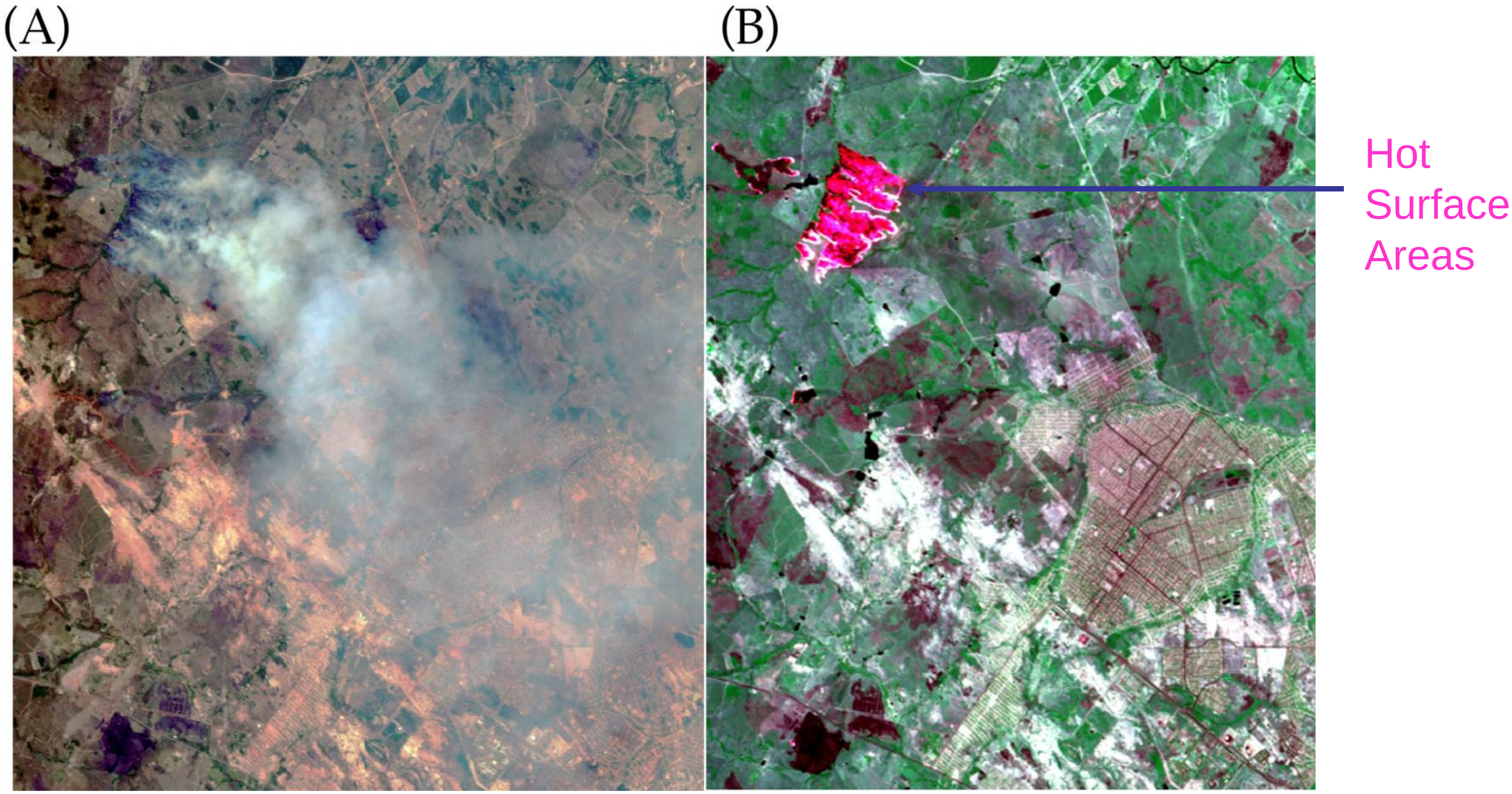

Smoke is seen in visible channel images, but disappears in the near-IR channel images. Smoke particle size is ~0.1 – 0.2 μm.

Atmospheric Gas Absorption

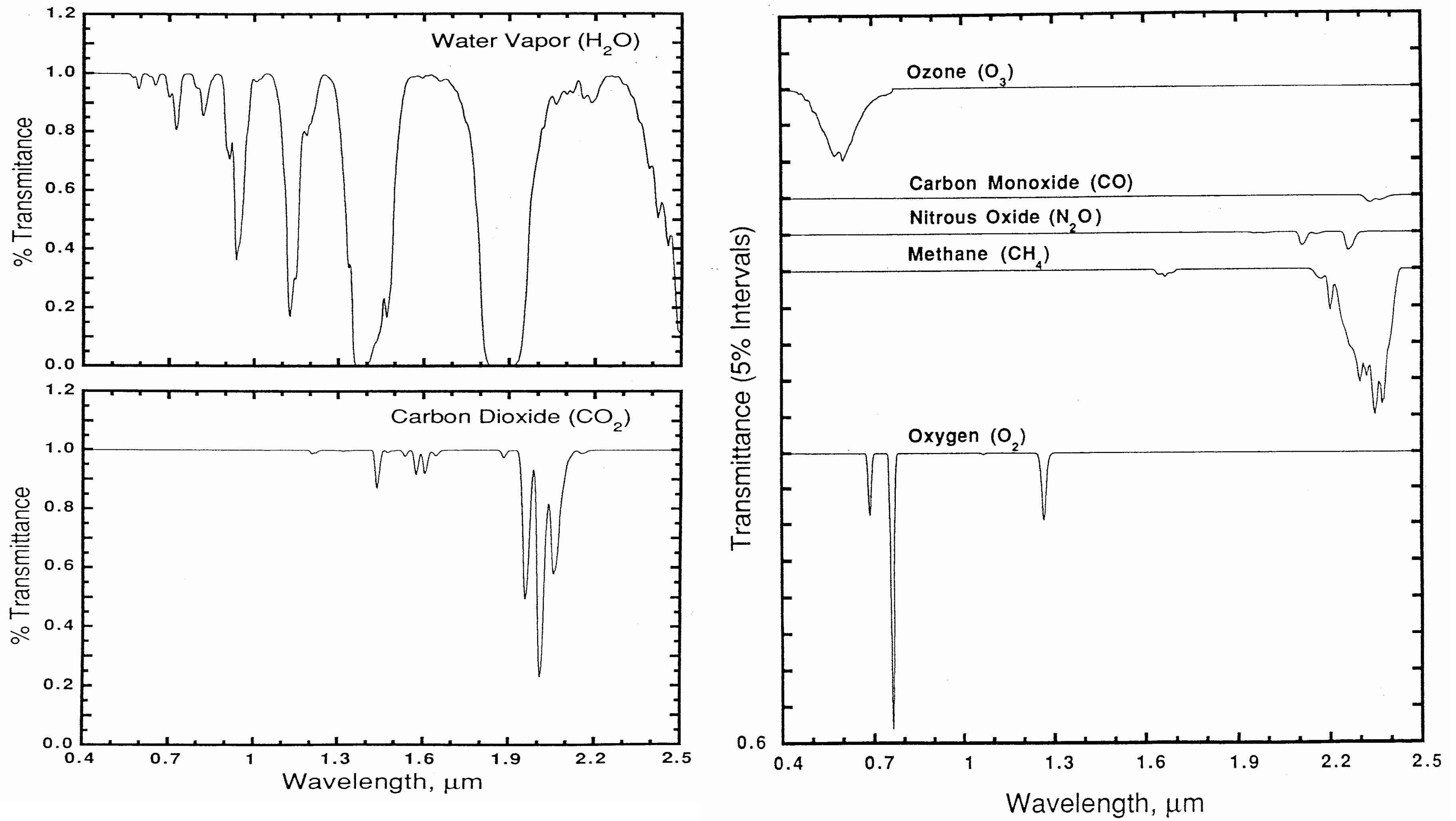

Water Vapor & Vegetation Liquid Water Derivation Using Spectrum-Matching or Channel Ratio Techniques

Spectrum-Matching
(a soil pixel)

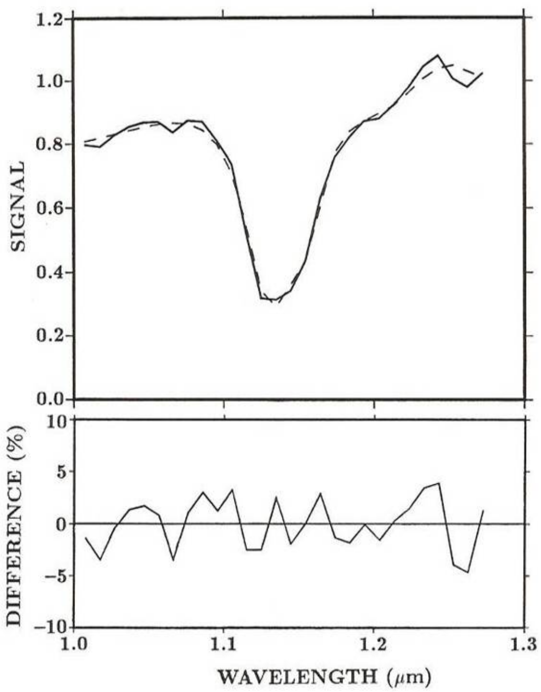

Spectrum-Matching
(green vegetation)

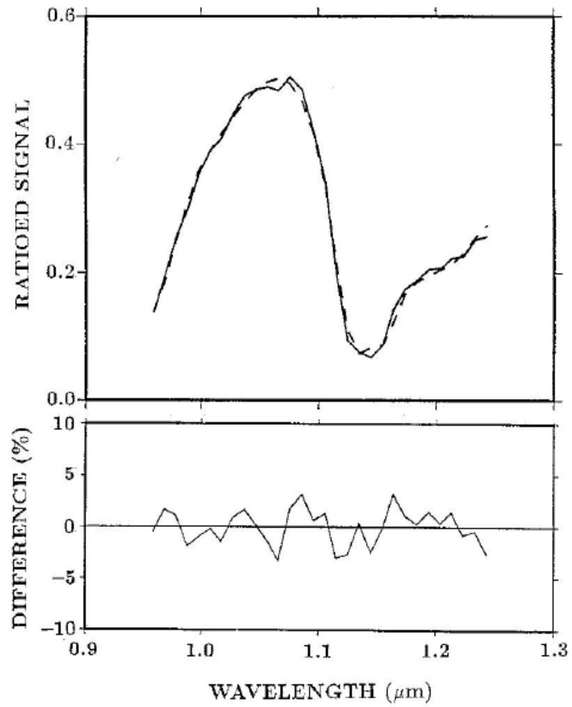

Channel Ratio

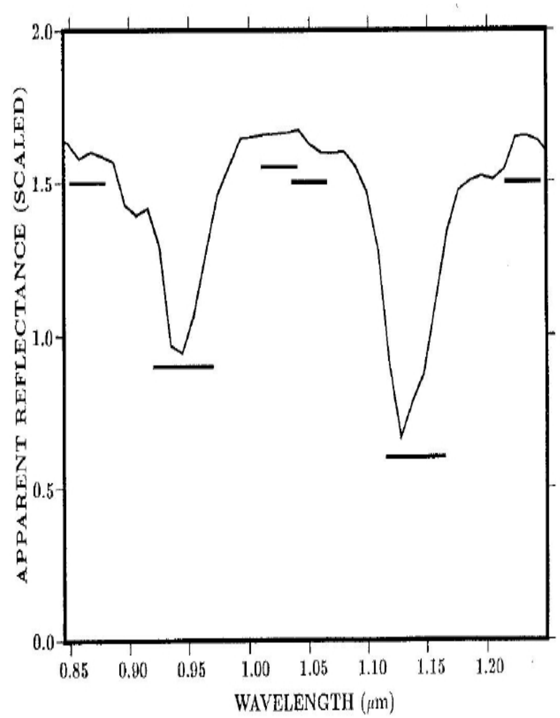

The sensitivity of the 0.94- and 1.14-micron water vapor bands and the surface reflectance properties allow us to retrieve water vapor amount using either spectrum-matching or channel ratio techniques. The water vapor effects in the entire 0.4 – 2.5 micron range can then be modeled and removed properly.

The Atmosphere Removal Algorithm (ATREM)

- We developed the 1st model-based operational atmospheric correction algorithm in 1991 with software support from Ms. Kathy Heidebrecht. Researchers in geology, soil, and vegetation sciences were invited to test ATREM. Based on their feedback, ATREM was modified several times to increase its usability for scientists with limited atmospheric radiative transfer background. The code was publicly released in 1993.

- Sample input files were also released together with the ATREM source code. A user only needs to modify one input file to suit a specific hyperspectral data set (date, time, latitude, longitude, etc.).

- Radiative transfer modeling and retrievals were automated inside ATREM.

- The output data include a water vapor image and a three dimensional surface reflectance data cube (2D spatial + 1D spectral).

Equations and Definitions

The measured radiance at the satellite level can be expressed as:

$$L_{obs} = L_a + L_{sun}\, t\, \rho \qquad (1)$$

L_a: path radiance;
ρ : surface reflectance;
L_{sun}: solar radiance above the atmosphere;
t: *2-way transmittance for the Sun-surface-sensor path*

Define the satellite apparent reflectance as

$$\rho^*_{obs} = \pi\, L_{obs} / (\mu_0\, E_0) \qquad (2)$$

$$\rho^*_{obs} = T_g\, [\, \rho_a + t\, \rho / (1 - \rho\, s)\,] \qquad (3)$$

By inverting Eq. (3) for ρ, we get:

$$\rho = (\rho^*_{obs}/T_g - \rho^*_a) / [t + s\, (\rho^*_{obs}/T_g - \rho^*_a)\,] \qquad (4)$$

Gao, B.-C., K. H. Heidebrecht, and A. F. H. Goetz, Derivation of scaled surface reflectances from AVIRIS data, *Remote Sens. Env., 44*, 165-178, 1993.

Line-by-Line Water Vapor Transmittance at 0.5 cm^{-1} Sampling

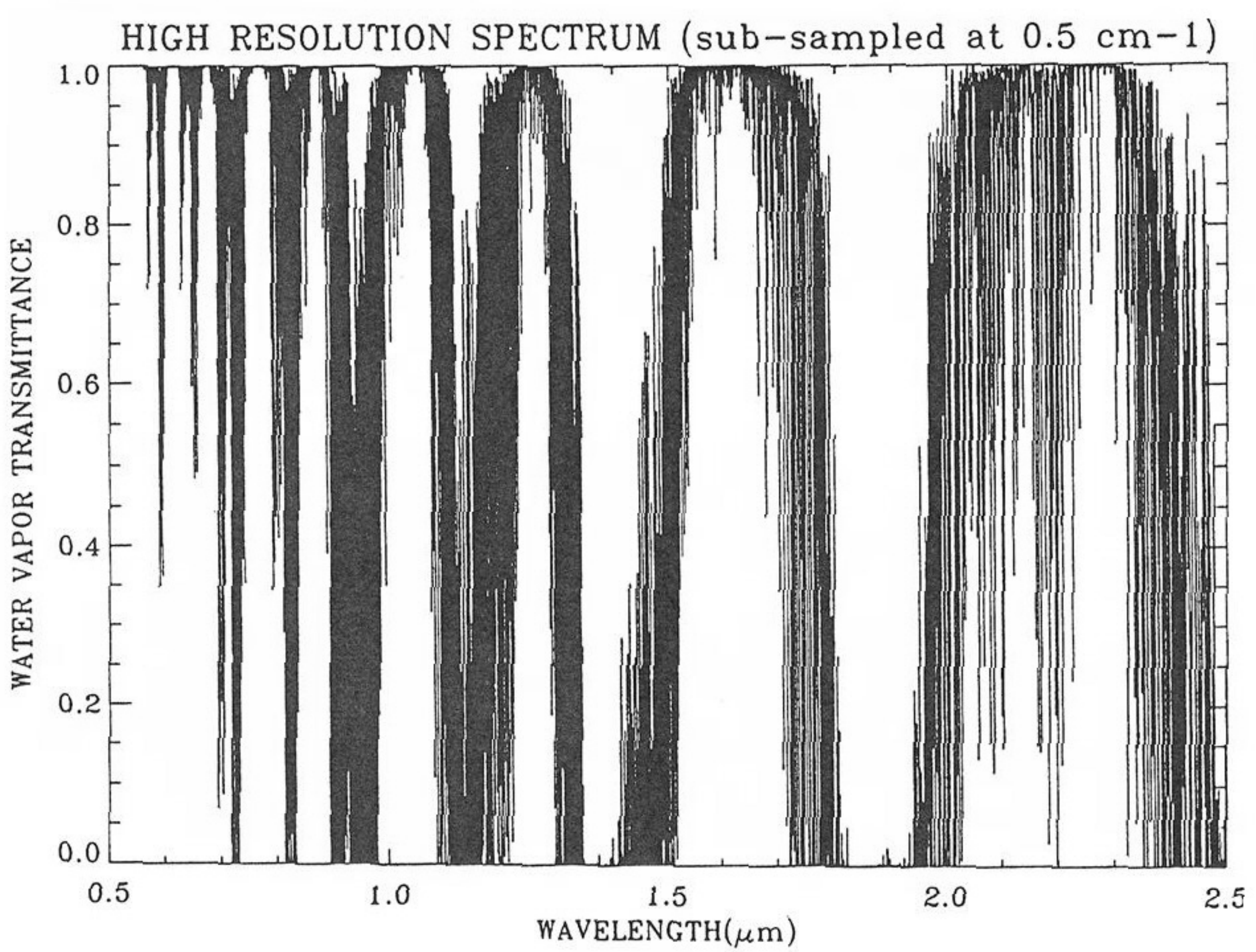

The line-by-line data can be smoothed to lower resolution data and to match the spectral resolution of almost all imaging spectrometer data.

SAMPLE REFLECTANCE RETRIEVALS OVER MINERAL

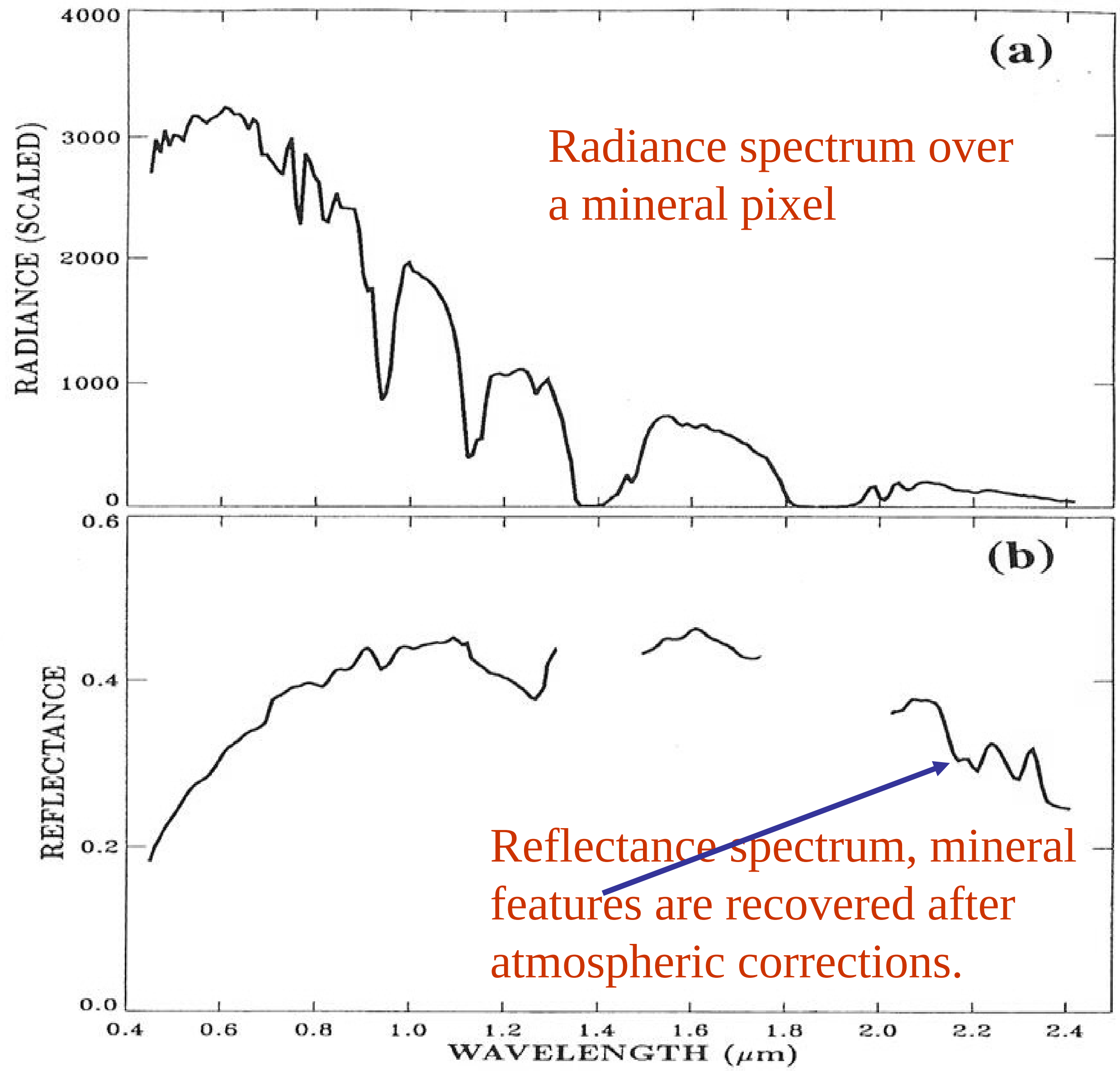

MINERAL MAPPING USING ATREM OUTPUT
by Scientists at USGS in Denver, Colorado

RGB Image (Cuprite, NV)

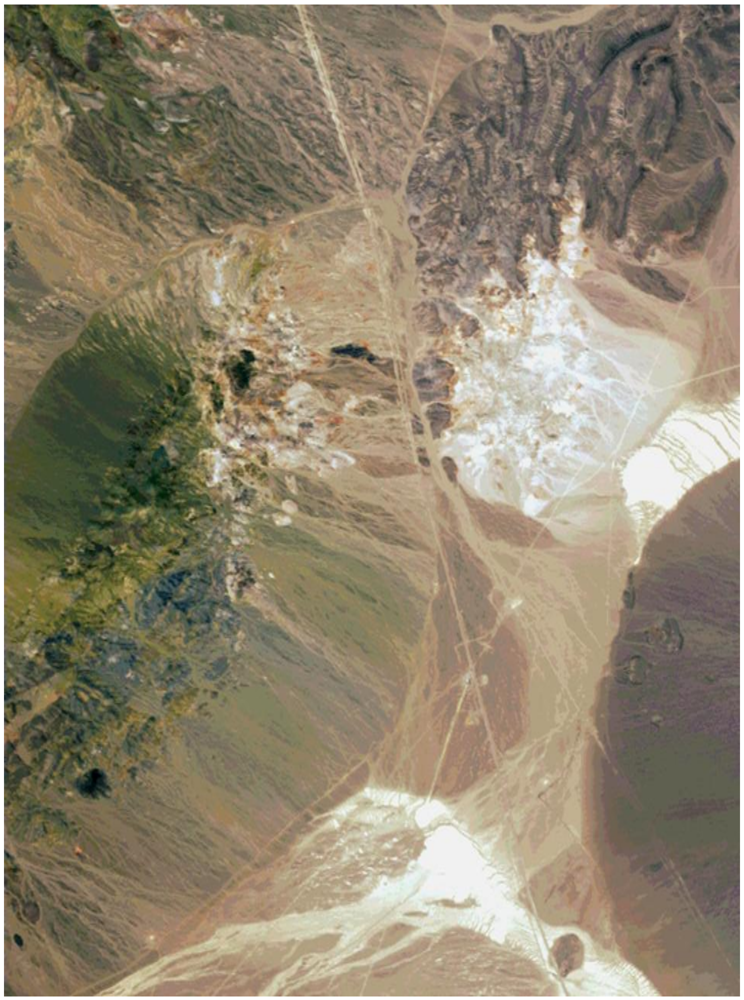

USGS Mineral Map, ~11x18 km

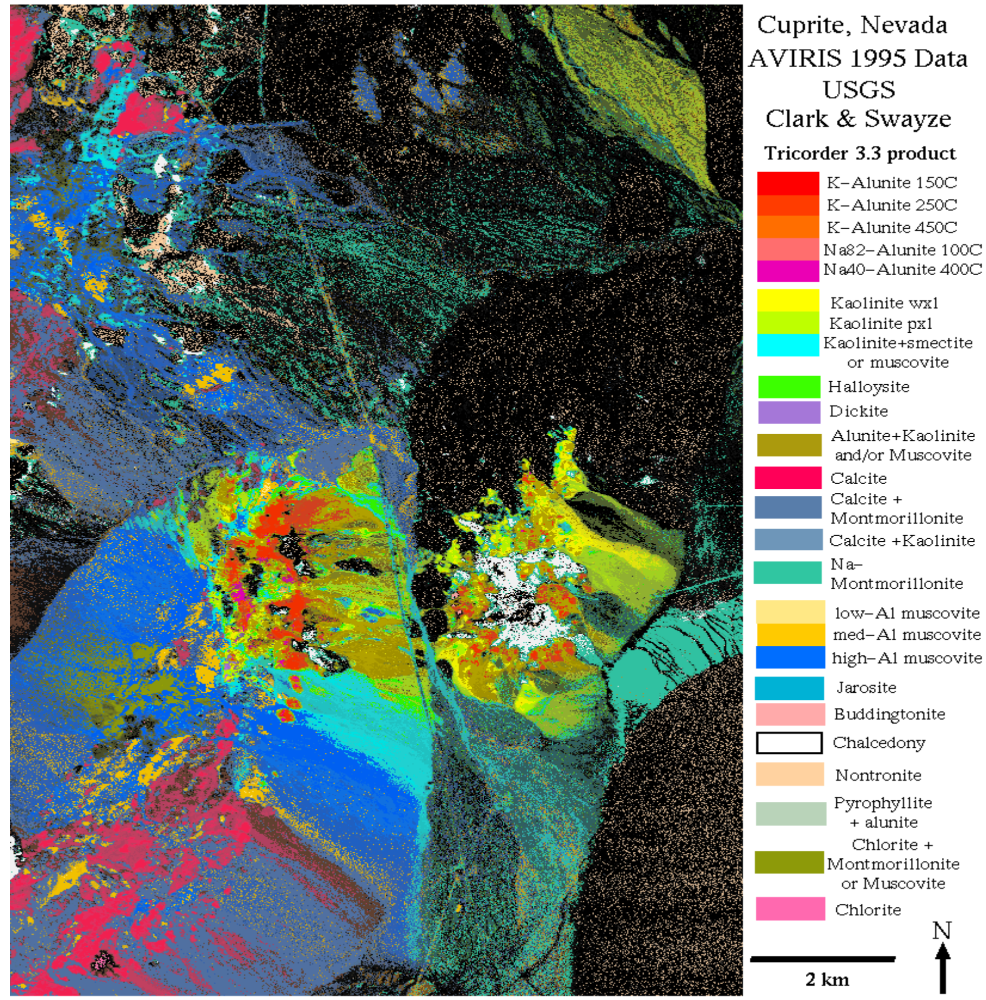

SAMPLE REFLECTANCE RETRIEVALS WITH ATREM

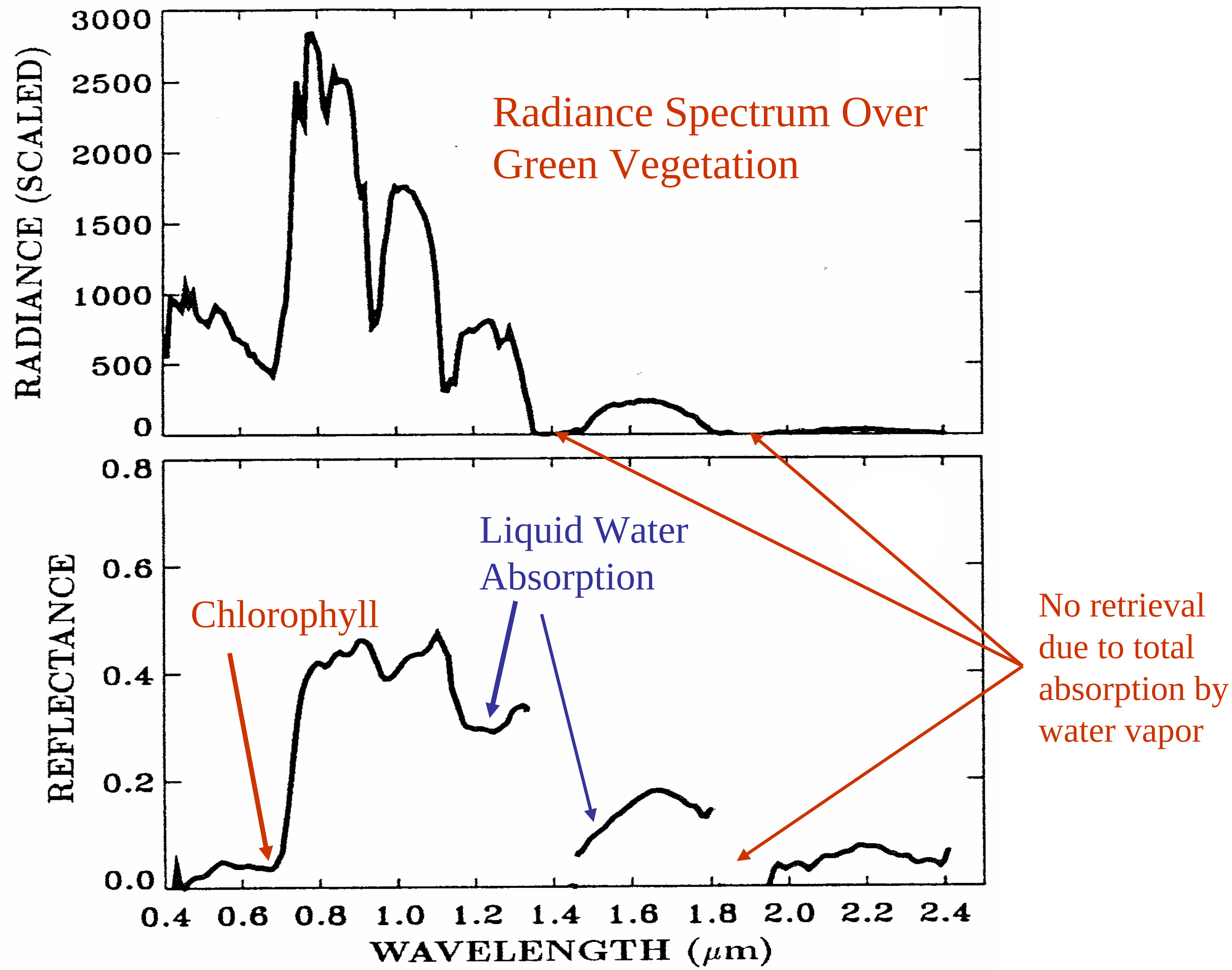

Vegetation Functional Type Analysis, Santa Barbara, CA

Dar Roberts, et al, UCSB

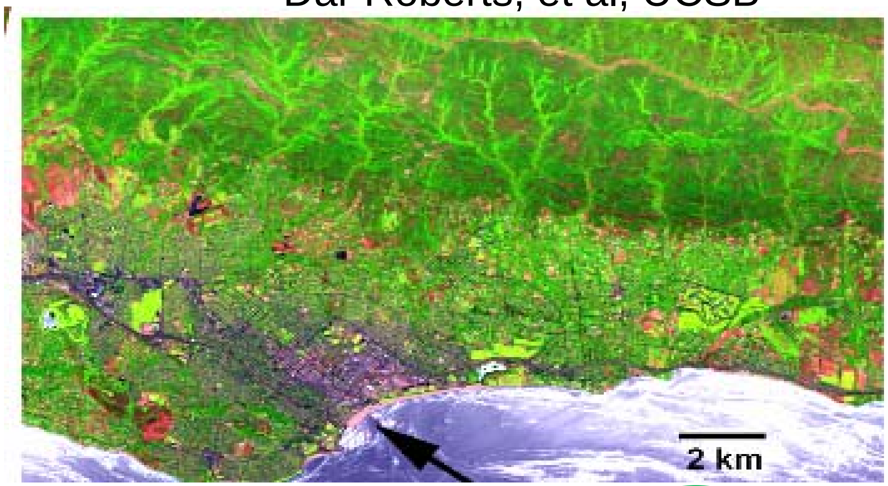

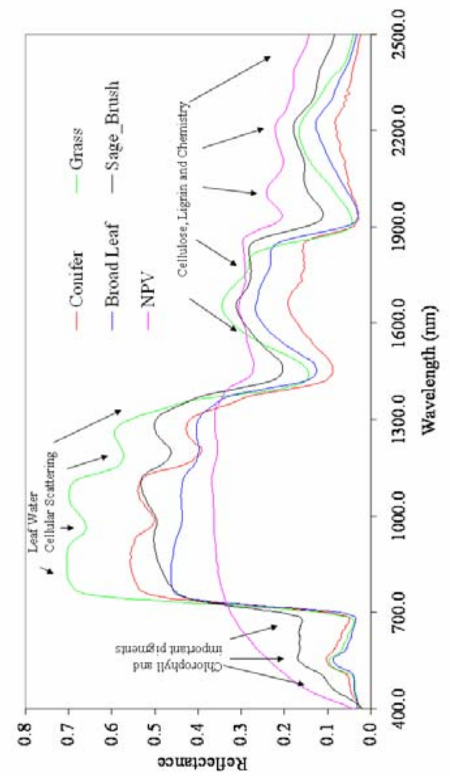

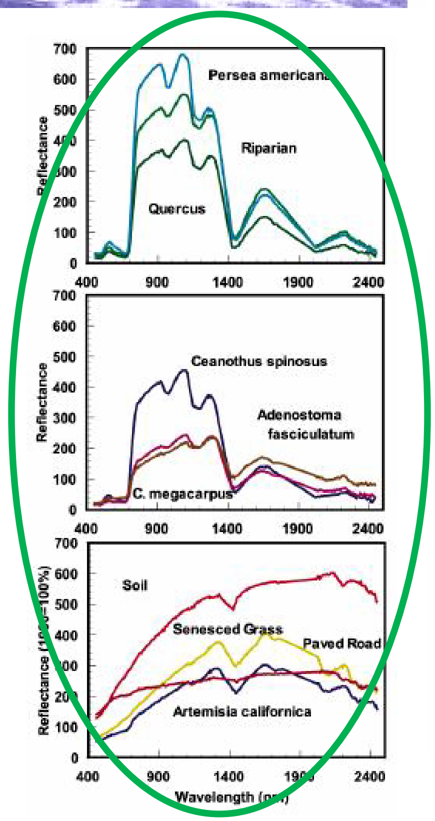

MESMA Species Type 90% accurate

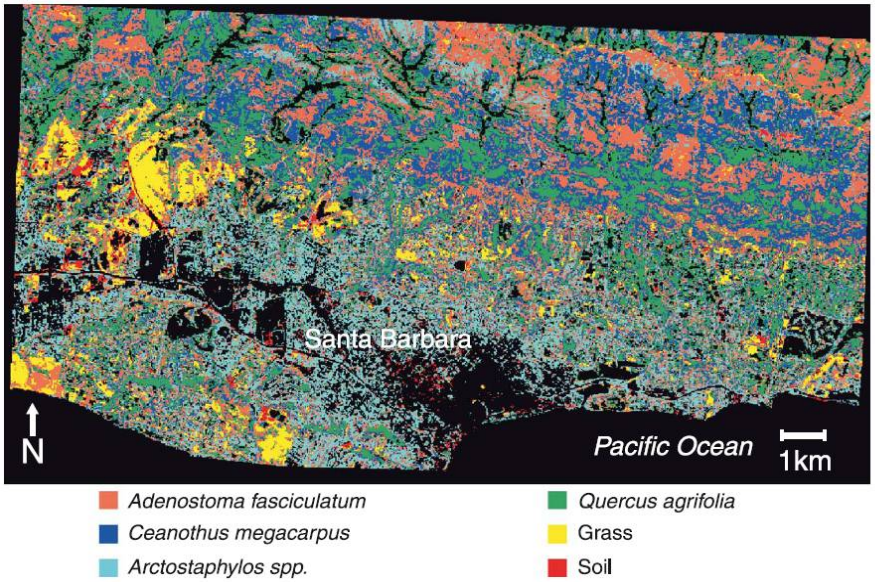

Species Fractional Cover

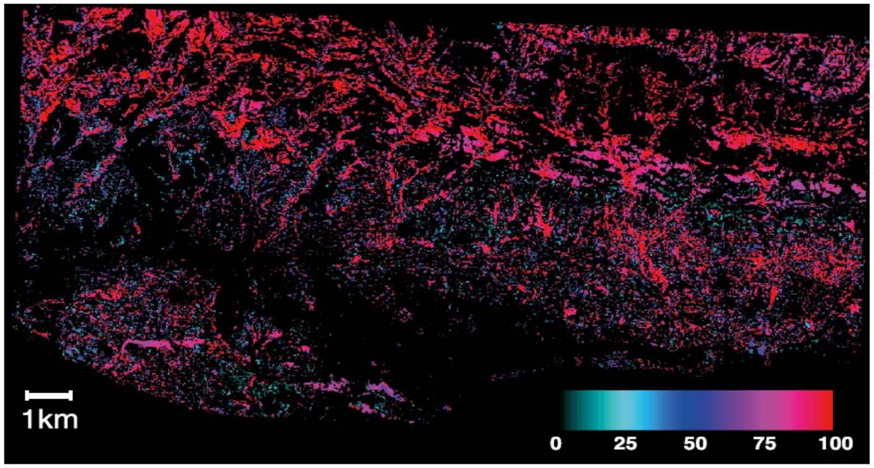

Part II: Ocean Version of the Atmospheric Correction Algorithm

Atmospheric Correction Over Water

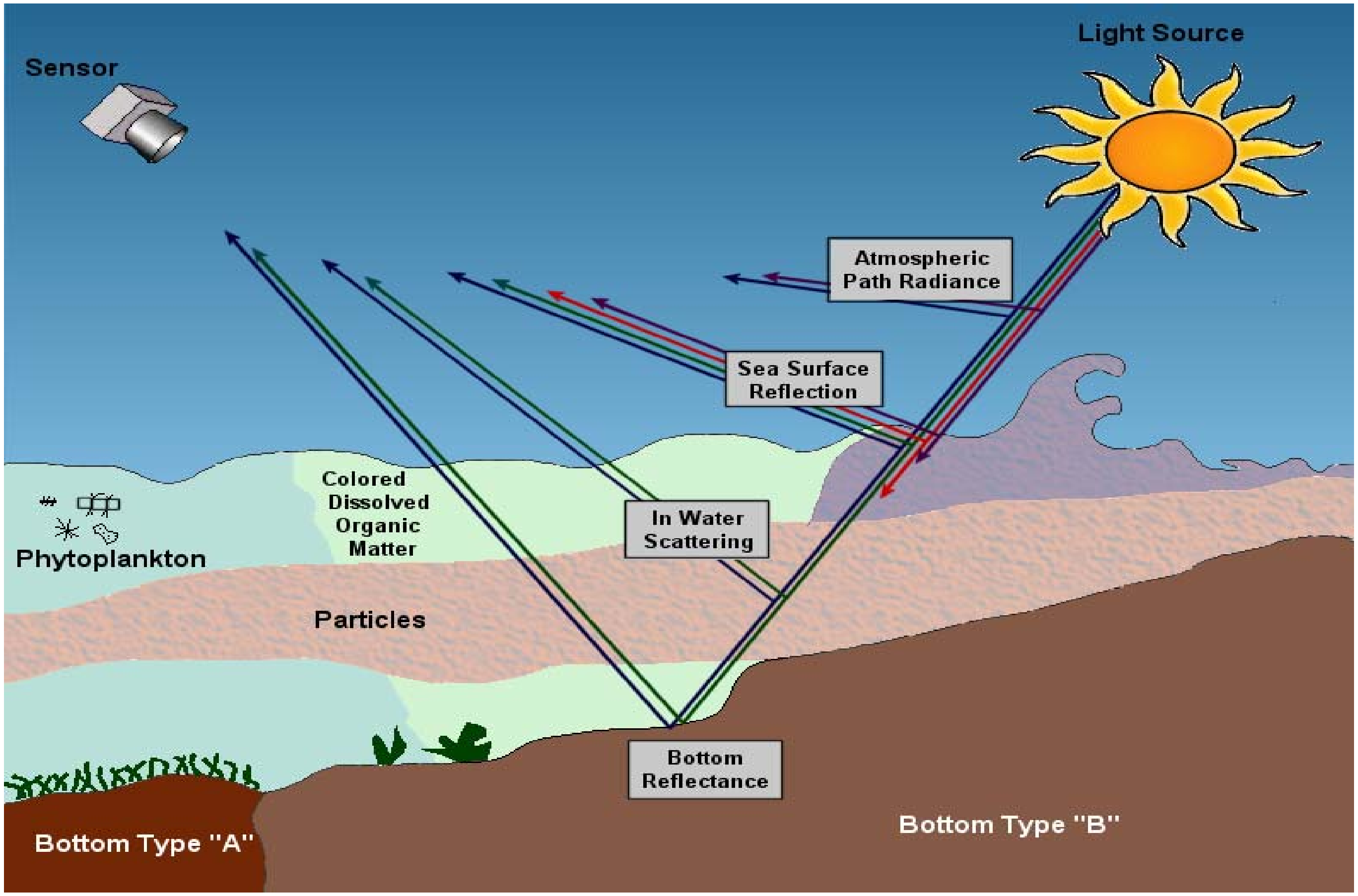

Over the dark water surfaces, ~90% of satellite radiances come from the atmosphere, and ~10% come from water. Very accurate atmospheric corrections are required in order to derive the useful water leaving reflectances. The specular reflection at the air/water interface introduces additional complications for modeling.

An AVIRIS Spectrum Over A Water Pixel

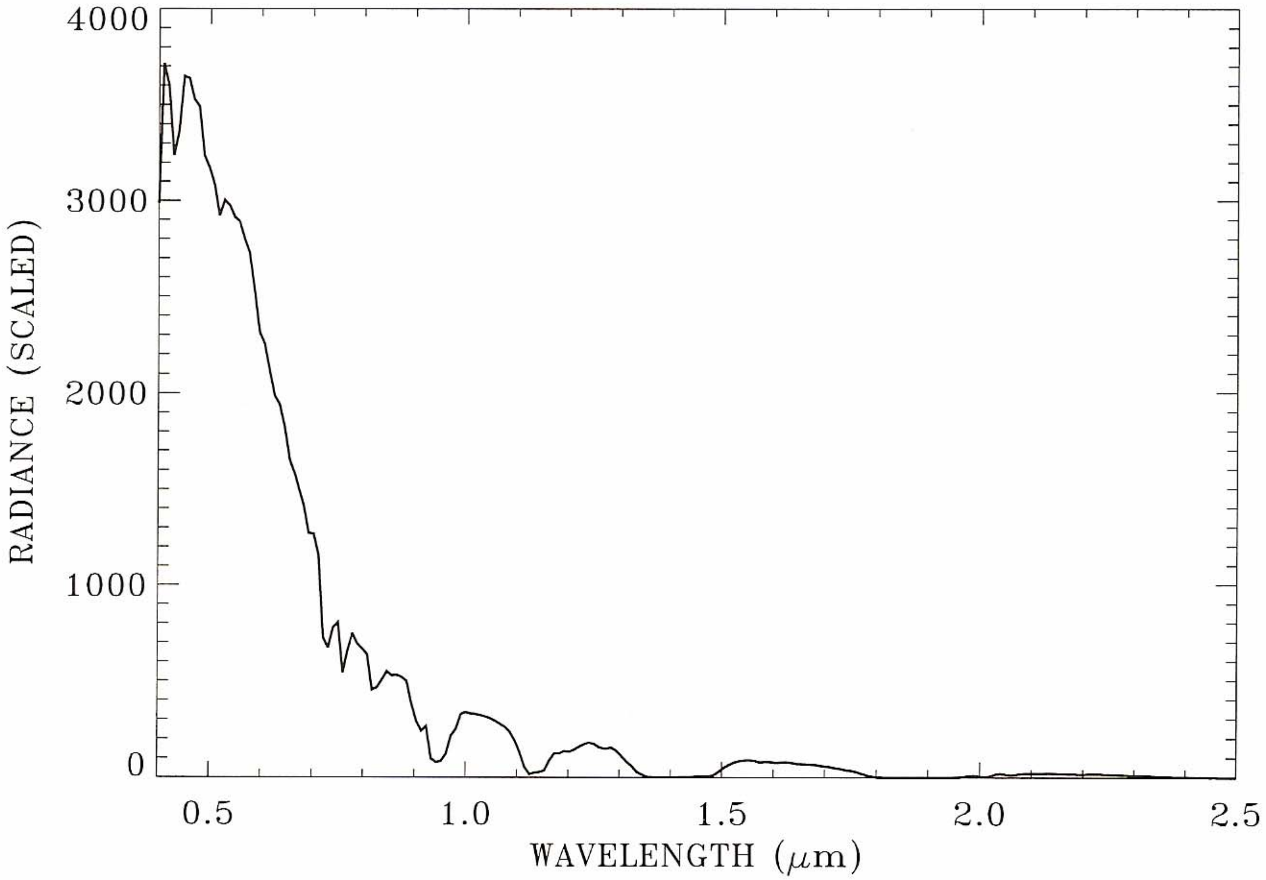

The radiances above one micron are very small.

Adopting R. Fraser Formulation

$$L_t = L_0(\lambda; \theta, \phi; \theta_0, \phi_0; z_{sen}, z_{sfc}\ ; \tau_a) +$$
$$L_{sfc}(\lambda; \theta, \phi; \theta_0, \phi_0; z_{sen}, z_{sfc}\ ; \tau_a; W)\ t(\lambda; \theta; z_{sen}, z_{sfc}\ ; \tau_a) +$$
$$L_w(\lambda; \theta, \phi; \theta_0, \phi_0; W; C)\ t'(\lambda; \theta; z_{sen}, z_{sfc}\ ; \tau_a)$$

L_t	=	measured radiance
L_0	=	path radiance (i.e., atmospheric scattering)
L_{sfc}	=	direct and diffuse radiance reflected off ocean surface
L_w	=	water (or ground) leaving radiance
t	=	diffuse + direct upward transmission
t'	=	diffuse upward transmission
τ_a	=	aerosol optical properties
W	=	wind speed
C	=	water column and bottom constituents
θ, ϕ	=	view zenith and azimuth angles
θ_0, ϕ_0	=	solar zenith and azimuth angles
z_{sen}, z_{sfc}	=	sensor and surface altitudes

Relevant Equations and Definitions

In the absence of gas absorption, the radiance at the satellite level is:

$$L_{obs} = L_0 + L_{sfc}\, t'_u + L_w\, t_u, \tag{1}$$

L_0: path radiance; L_w: water leaving radiance;
L_{sfc}: radiance reflected at water surface; t_u: *upward transmittance*

Define $$L_{atm+sfc} = L_0 + L_{sfc}\, t'_u \tag{2}$$

Eq. (1) becomes: $L_{obs} = L_{atm+sfc} + L_w\, t_u$ (3)

Multiply Eq. (3) by π and divide by $(\mu_0 E_0)$, Eq. (3) becomes:

$$\pi L_{obs} / (\mu_0 E_0) = \pi L_{atm+sfc} / (\mu_0 E_0) + \pi L_w\, t_d\, t_u / (\mu_0 E_0\, t_d) \tag{4}$$

Several reflectances are defined as:
Satellite apparent reflectance: $\rho^*_{obs} = \pi L_{obs} / (\mu_0 E_0)$, (5)

$$\rho^*_{atm+sfc} = \pi L_{atm+sfc} / (\mu_0 E_0), \tag{6}$$

Water leaving reflectance: $\boldsymbol{\rho_w = \pi L_w / (\mu_0 E_0\, t_d) = \pi L_w / E_d}$ **(7)**
Remote sensing reflectance: $\mathbf{R_{rs}} = \boldsymbol{\rho_w / \pi = L_w / E_d}$ **(7')**

Substitute Eqs (5) – (7) into Eq. (4): $\rho^*_{obs} = \rho^*_{atm+sfc} + \rho_w\, t_d\, t_u$ (8)

After consideration of gas absorption and multiple reflection between the atmosphere and surface and with further manipulation, we can get:

$$\rho_w = (\rho^*_{obs}/T_g - \rho^*_{atm+sfc}) / [t_d\, t_u + s\, (\rho^*_{obs}/T_g - \rho^*_{atm+sfc})] \tag{11}$$

Gao, B.-C., M. J. Montes, Z. Ahmad, and C. O. Davis, Atmospheric correction algorithm for hyperspectral remote sensing of ocean color from space, Appl. Opt., 39, 887-896, February 2000.

Simulation of Aerosol Effects

Using Ahmad and Fraser RT code to generate lookup tables

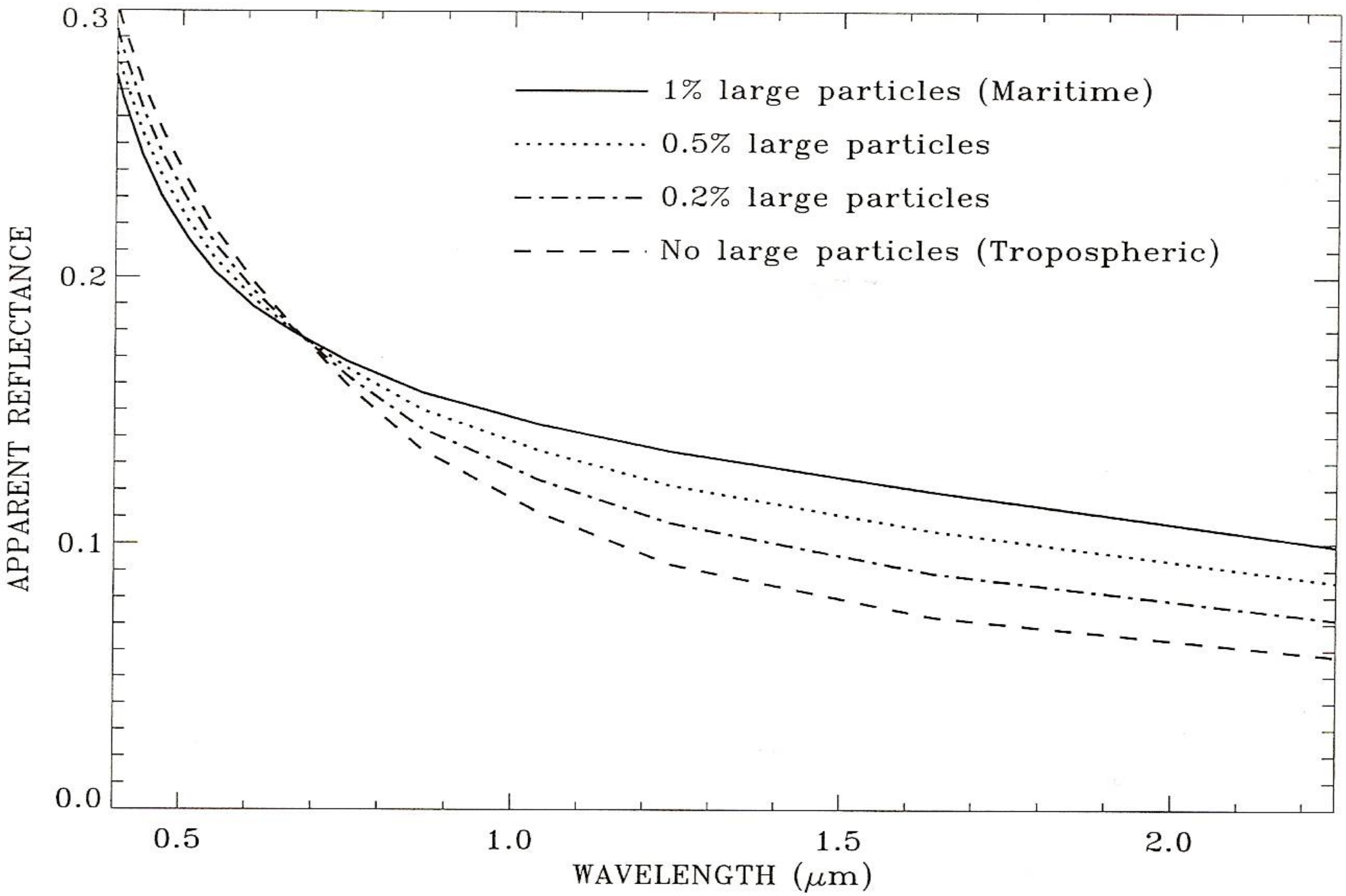

Aerosol optical depth at 0.55 micron is 0.7

Simulation of Sunglint Effects

Using Ahmad and Fraser RT code to generate lookup tables

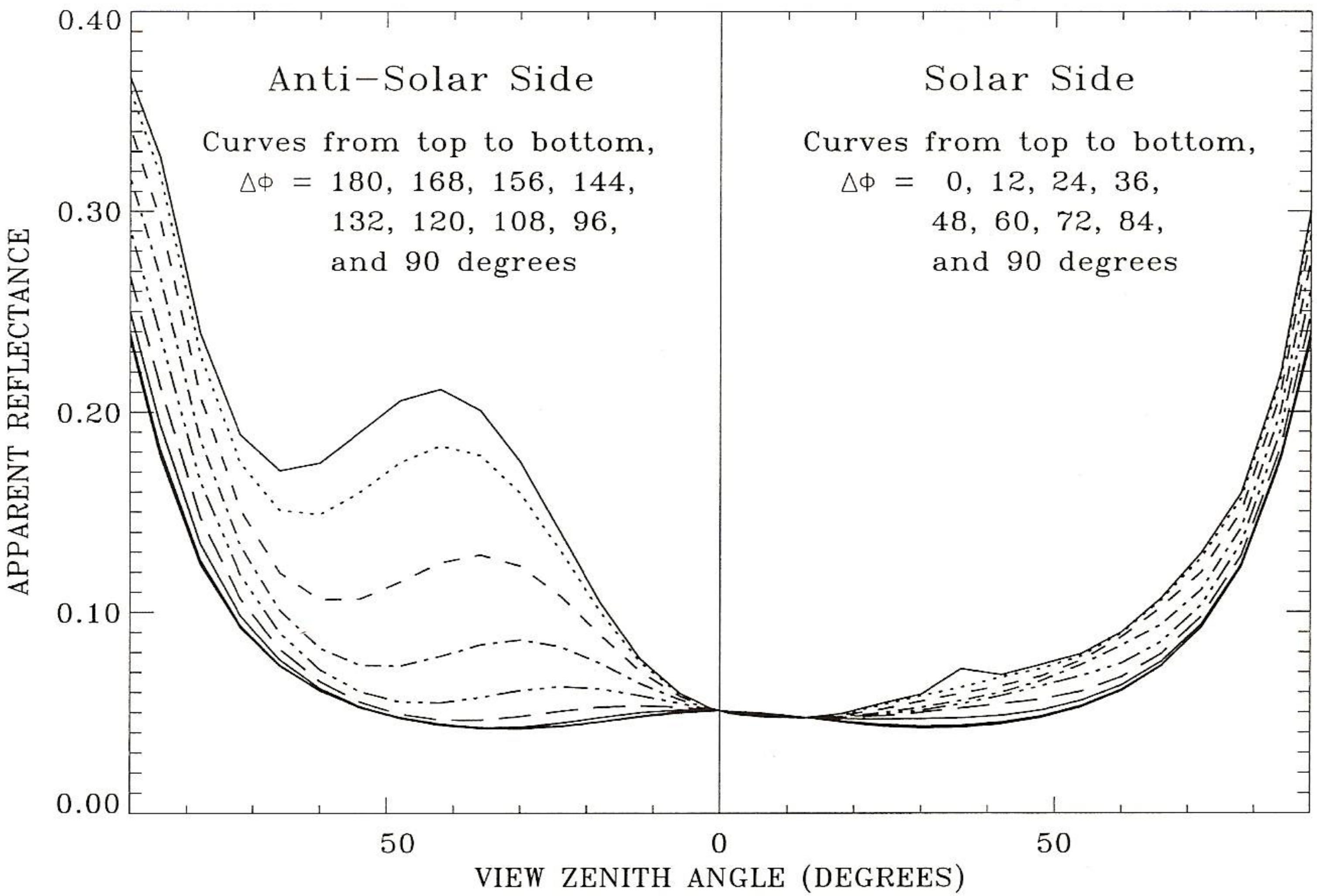

Wavelength: 0.61 micron

Coastal Waters Are Dark Above 0.86 Micron (AVIRIS Norfork Images)

RGB (0.66, 0.55, 0.47 μm)

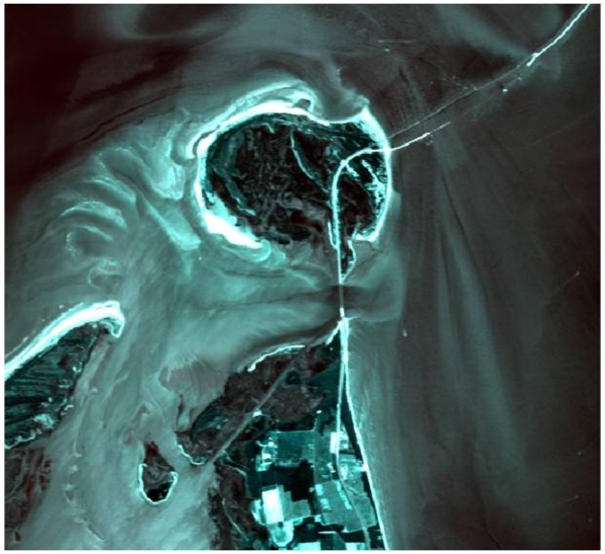

0.55-μm

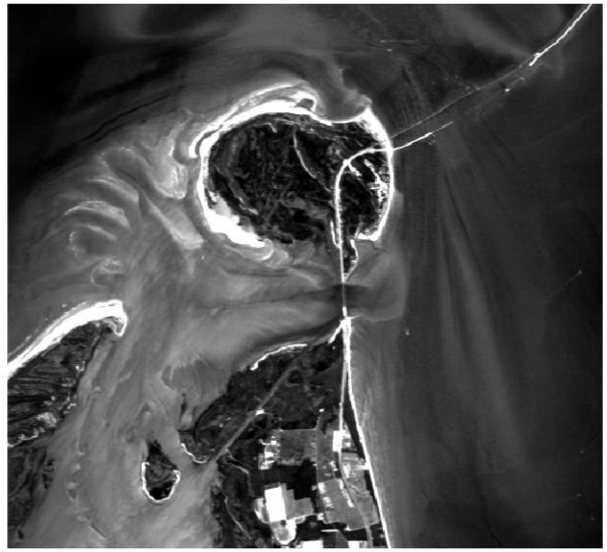

0.66-μm

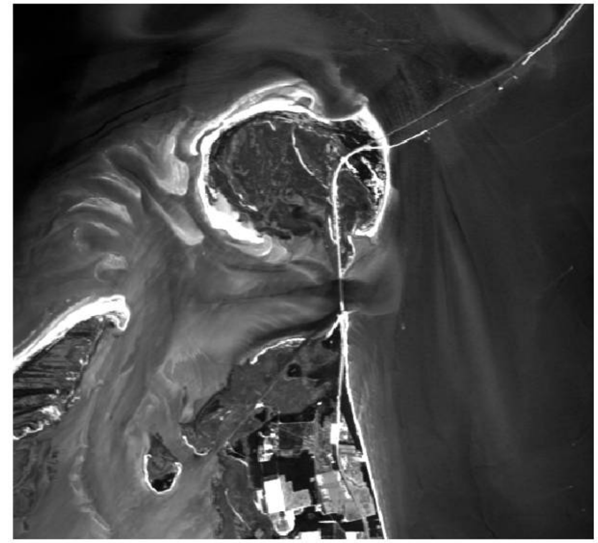

0.75-μm

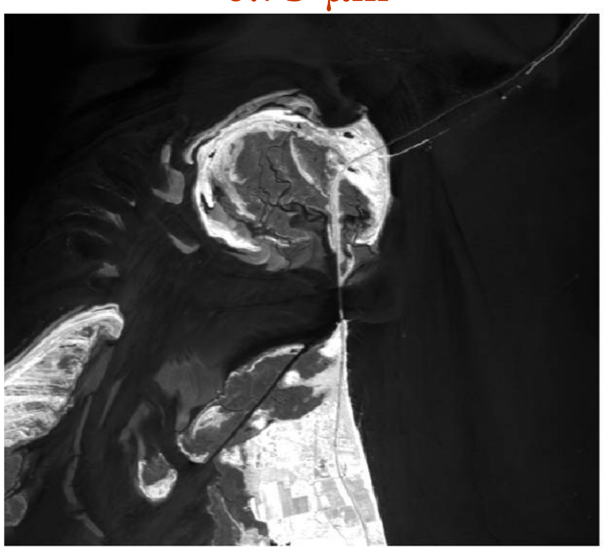

0.86-μm

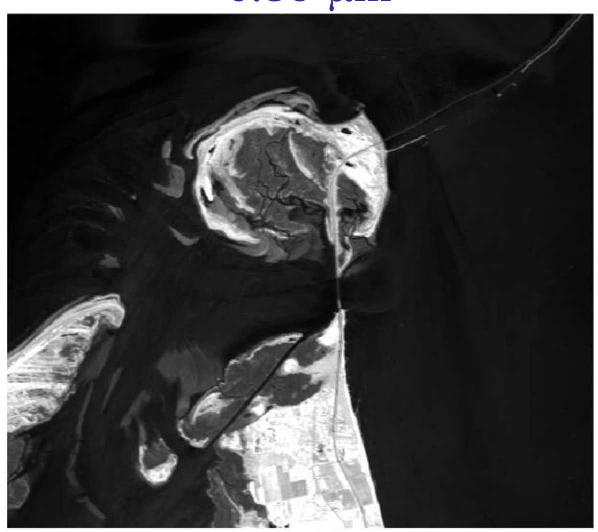

1.02-μm

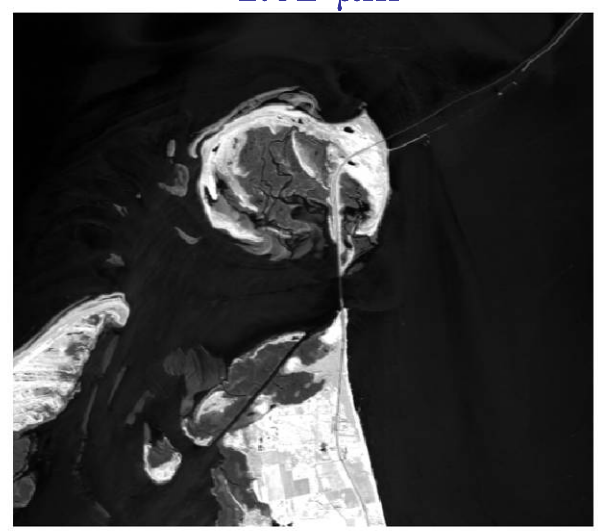

Atmospheric Correction for Water Surfaces

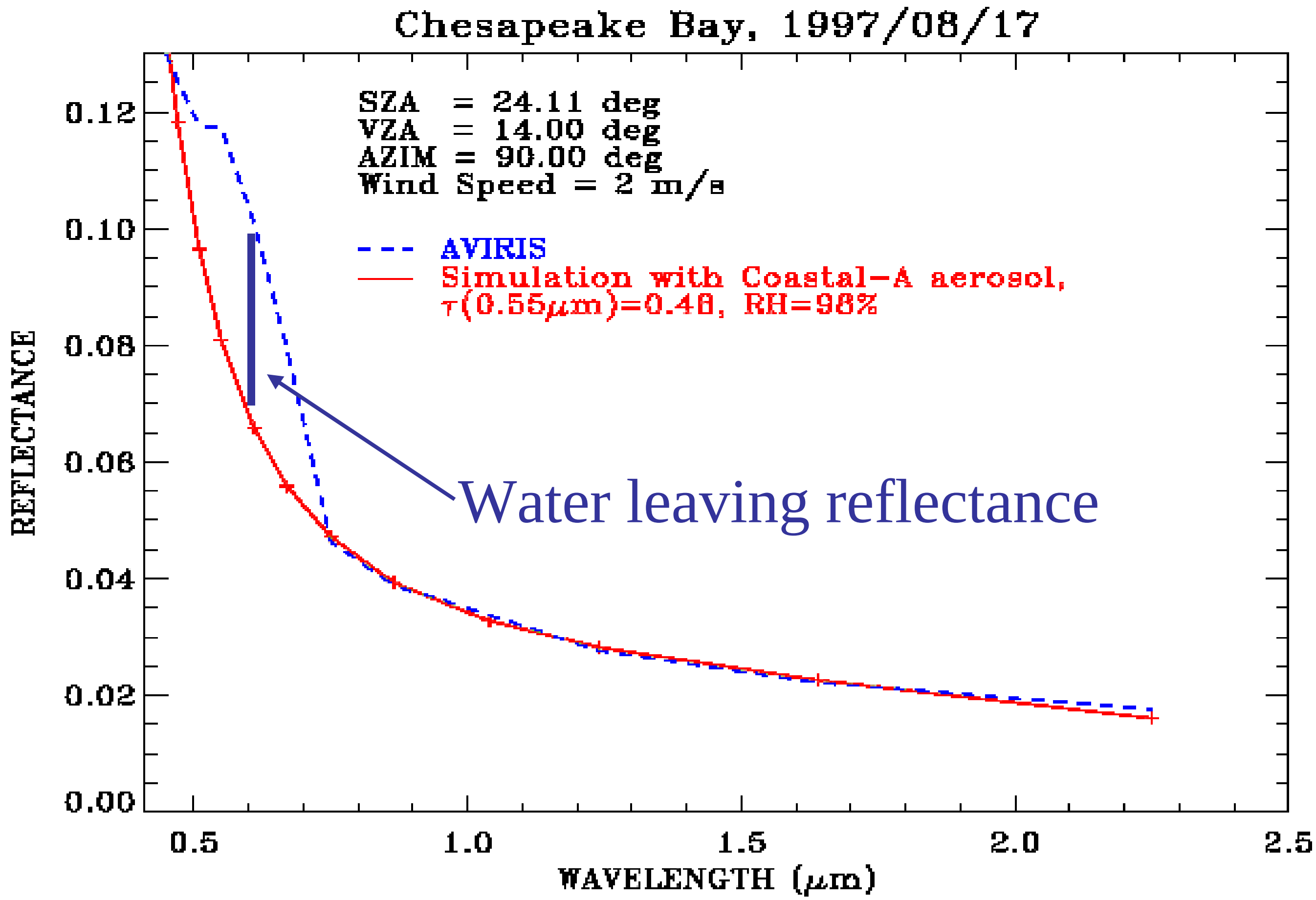

Channels at 0.86 and longer wavelengths are used to estimate atmospheric effects, and then extrapolate to the visible region. The differences between the two curves above are proportional to water leaving reflectances.

Sample Retrievals Over Water (continued)

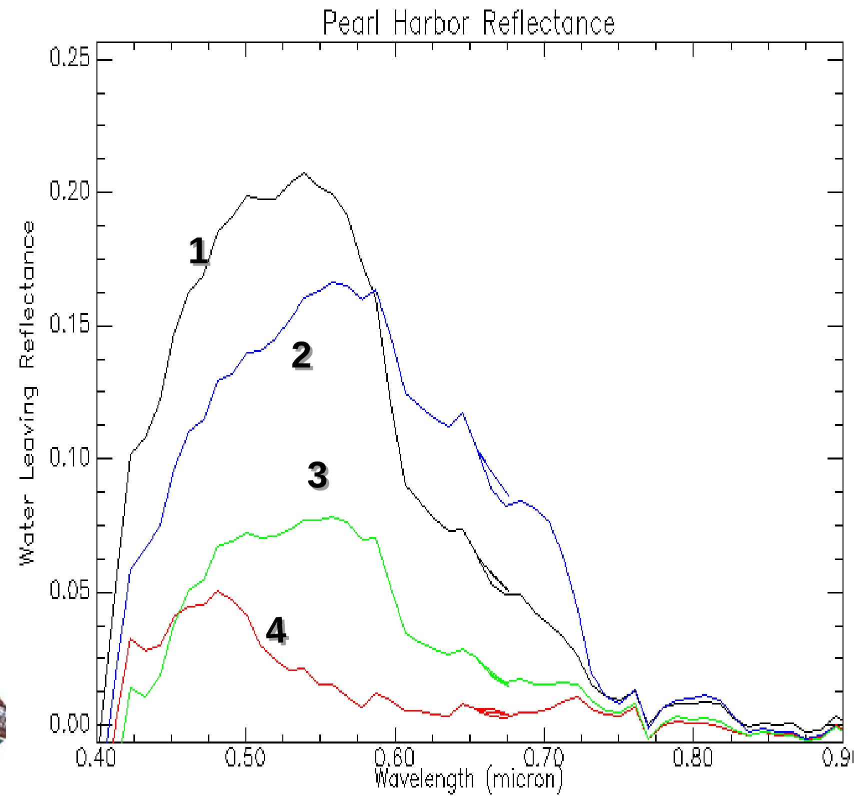

AVIRIS image of Pearl Harbor, HI April 12, 2000. Data processed to reflectance using Tafkaa.

Shallow Sandy Areas

AVIRIS

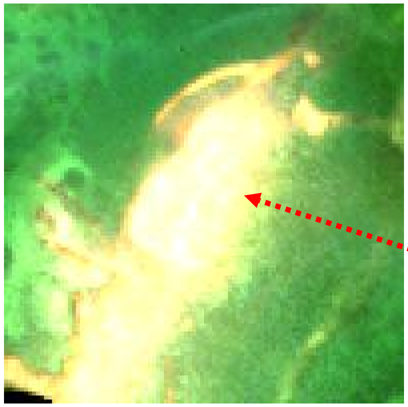

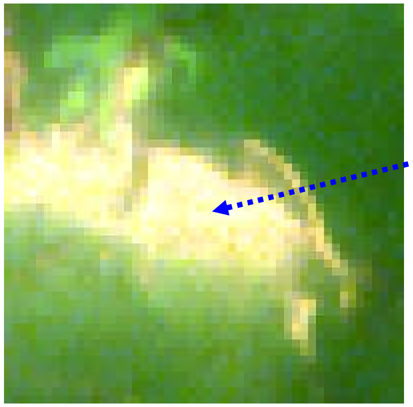

Hyperion

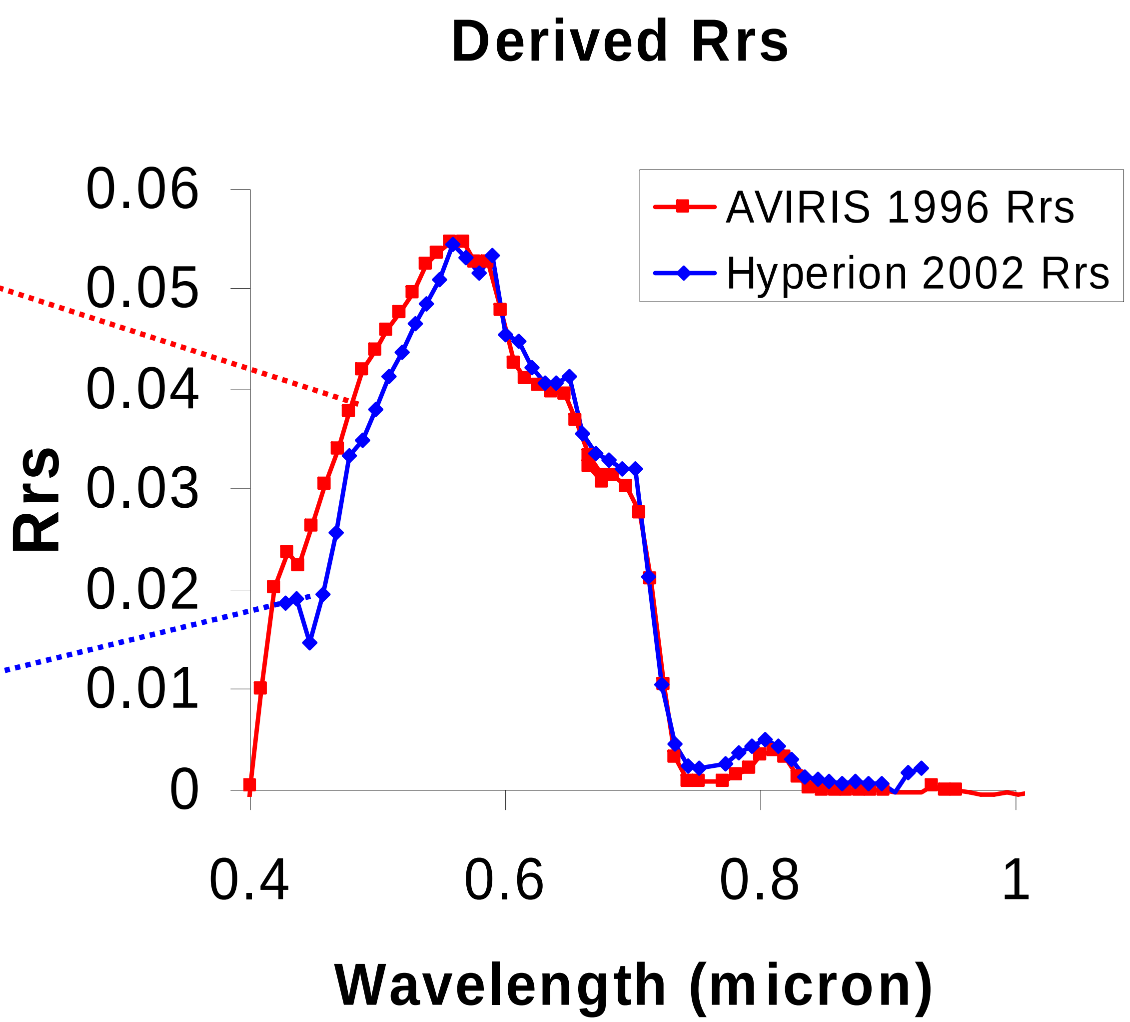

Sample Retrievals Over Water

Aircraft PHILLS data for Great Bay, NJ, from 2.6 km altitude

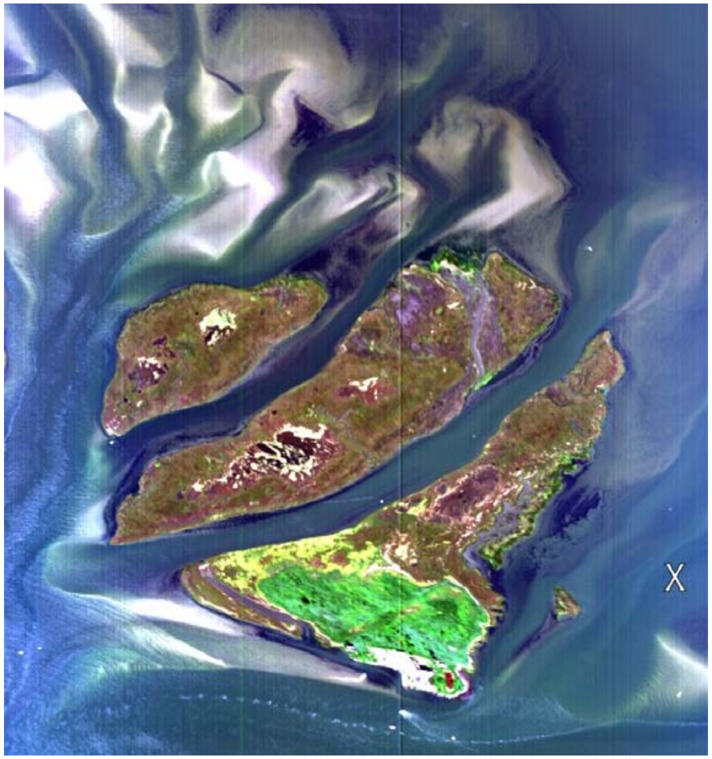

PHILLS image from the 2001 LEO-15 deployment (39 31 05 N and 74 20 47 W, 14:18 GMT, 31 July 2001.)

Lambertian reflectance of water-leaving radiance

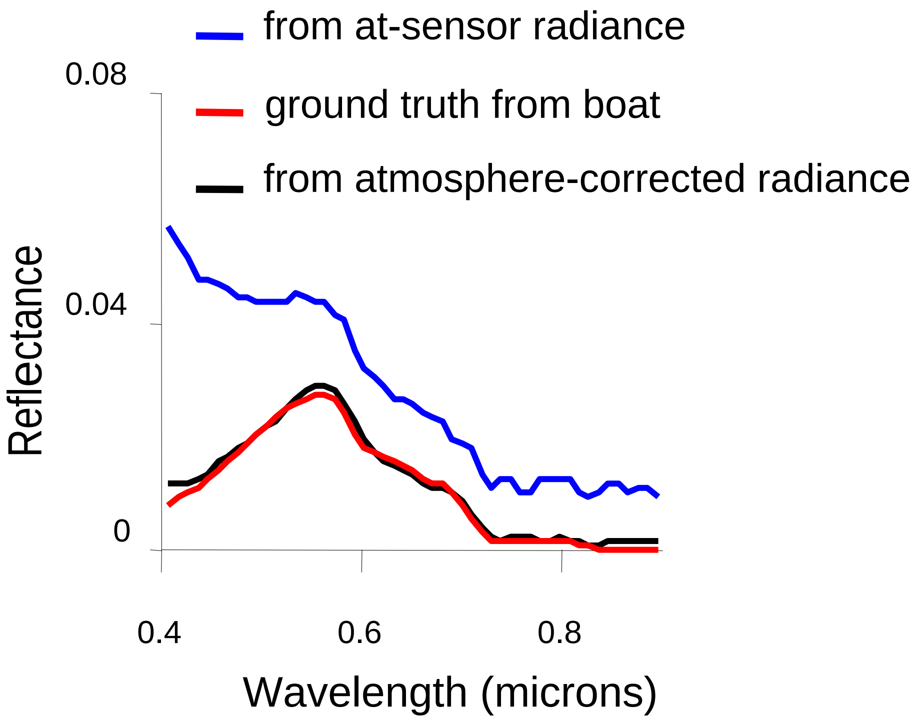

Remote Sensing of Environment 113 (2009) S17–S24

Contents lists available at ScienceDirect

Remote Sensing of Environment

journal homepage: www.elsevier.com/locate/rse

Atmospheric correction algorithms for hyperspectral remote sensing data of land and ocean

Bo-Cai Gao [a,*], Marcos J. Montes [a], Curtiss O. Davis [b], Alexander F.H. Goetz [c]

[a] Remote Sensing Division, Naval Research Laboratory, Washington, DC 20375 USA
[b] College of Oceanic and Atmospheric Sciences, Oregon State University, Corvallis, OR 97331 USA
[c] Analytical Spectral Devices, Inc., 5335 Sterling Drive, Boulder, CO 80301 USA

A R T I C L E I N F O

Article history:
Received 5 January 2007
Received in revised form 7 November 2007
Accepted 9 December 2007

Keywords:
Hyperspectral
Imaging spectrometer
Atmospheric correction
Remote sensing

A B S T R A C T

Hyperspectral imaging data have been collected with different types of imaging spectrometers from aircraft and satellite platforms since the mid-1980s. Because the solar radiation on the sun-surface-sensor path in the 0.4–2.5 μm visible and near-IR spectral regions is subject to absorption and scattering by atmospheric gases and aerosols, the hyperspectral imaging data contains atmospheric effects. In order to use hyperspectral imaging data for quantitative remote sensing of land surfaces and ocean color, the atmospheric effects must be removed. Over the years, atmospheric correction algorithms have evolved from the earlier empirical line method and the flat field method to more recent methods based on rigorous radiative transfer modeling approaches. Here, a review of hyperspectral atmospheric correction techniques is presented. Issues related to spectral smoothing are discussed. Suggestions for improvements to the present atmospheric correction

Current Status of the Algorithms

- At present, both the land and ocean version of the algorithms work reasonably well under typical atmospheric conditions.

- However, in the presence of absorbing aerosols, the model tends to overestimate the atmospheric contribution to the upwelling radiance, resulting in inferred surface reflectances which are biased low (even negative) in the blue region of the spectrum. Problem has been most prevalent in:
    - US east coastal areas
    - Desert regions.

The Needed Algorithm Upgrades

- Upgrades to our previously developed atmospheric correction algorithms are needed now, particularly in view of major advances in aerosol models. Specific upgrades include
    - Incorporation of absorbing aerosol models
    - Incorporation of UV channels (380 nm, 400 nm)
- Validation work with updated atmospheric correction Level 2 algorithms
- It is expected HyspIRI Level 2 algorithms with be developed based on this radiative transfer foundation and will be refined and optimized and validated for the global HyspIRI Mission

.

BACKUP SLIDES

Part III: Thin Cirrus Detection & Corrections

An Example of Cirrus Detection Using The High Spatial Resolution (20 m) AVIRIS Data

(A) VISIBLE

(B) 1.38 µm

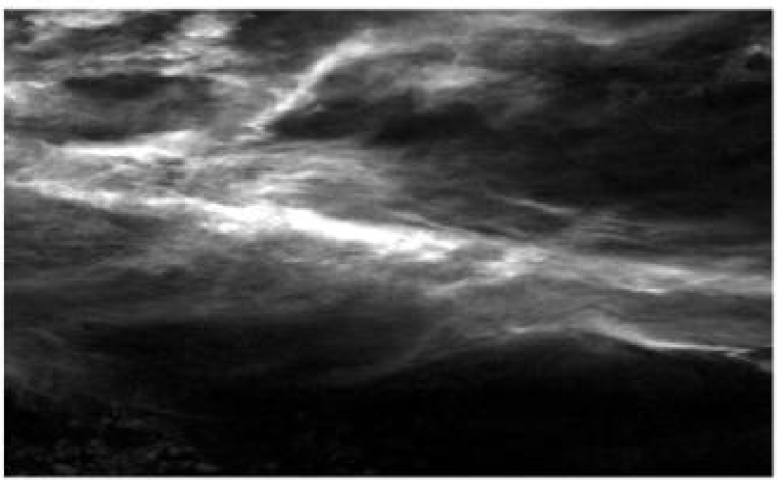

(C) 1.88 µm

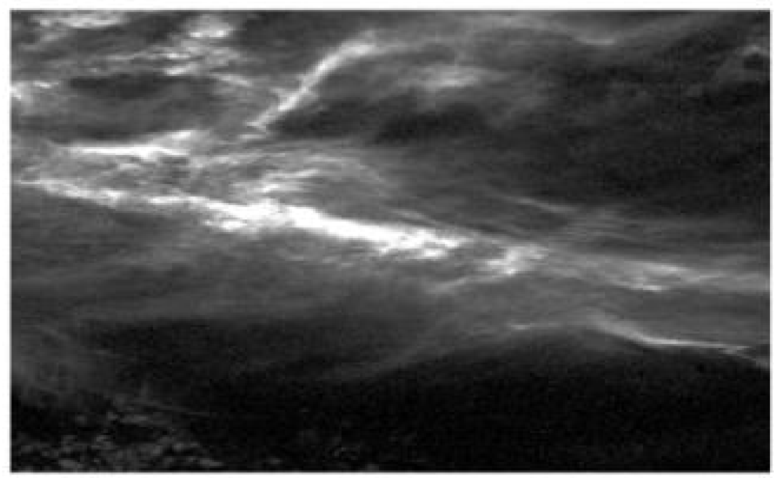

Examples of AVIRIS Spectra Over Cirrus & Clear Land Areas

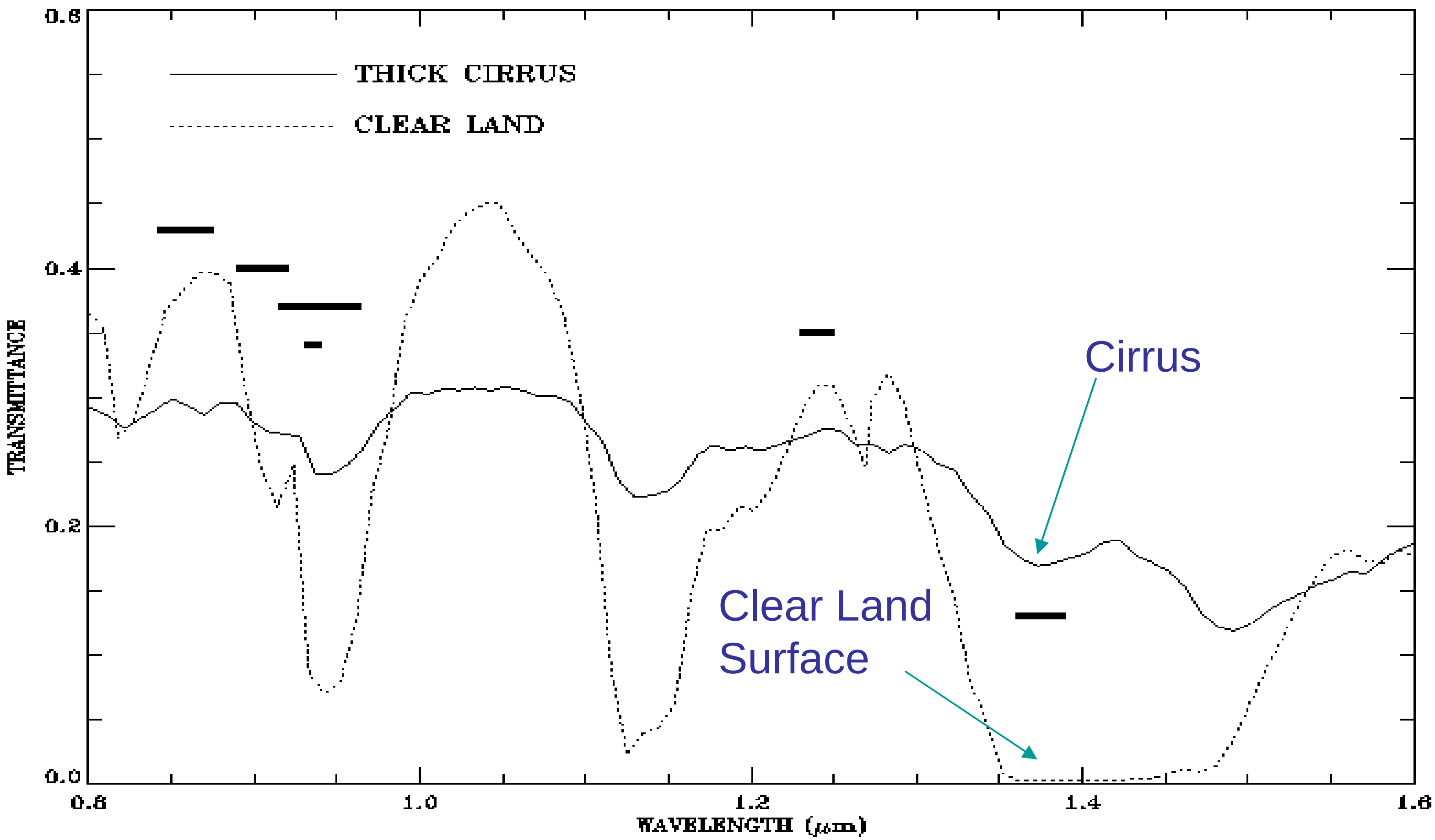

Under normal atmospheric conditions, AVIRIS channels near 1.38 micron do not detect radiances over clear pixels because of strong water vapor absorption at lower atmosphere. However, when cirrus clouds (typically at 8 km or higher) are present, these channels receive solar radiation scattered by the upper level cirrus clouds. As a result, thin cirrus clouds are easily detected with the channels near 1.38 micron.

Cirrus Corrections

AVIRIS data acquired over Bowie, MD in summer 1997

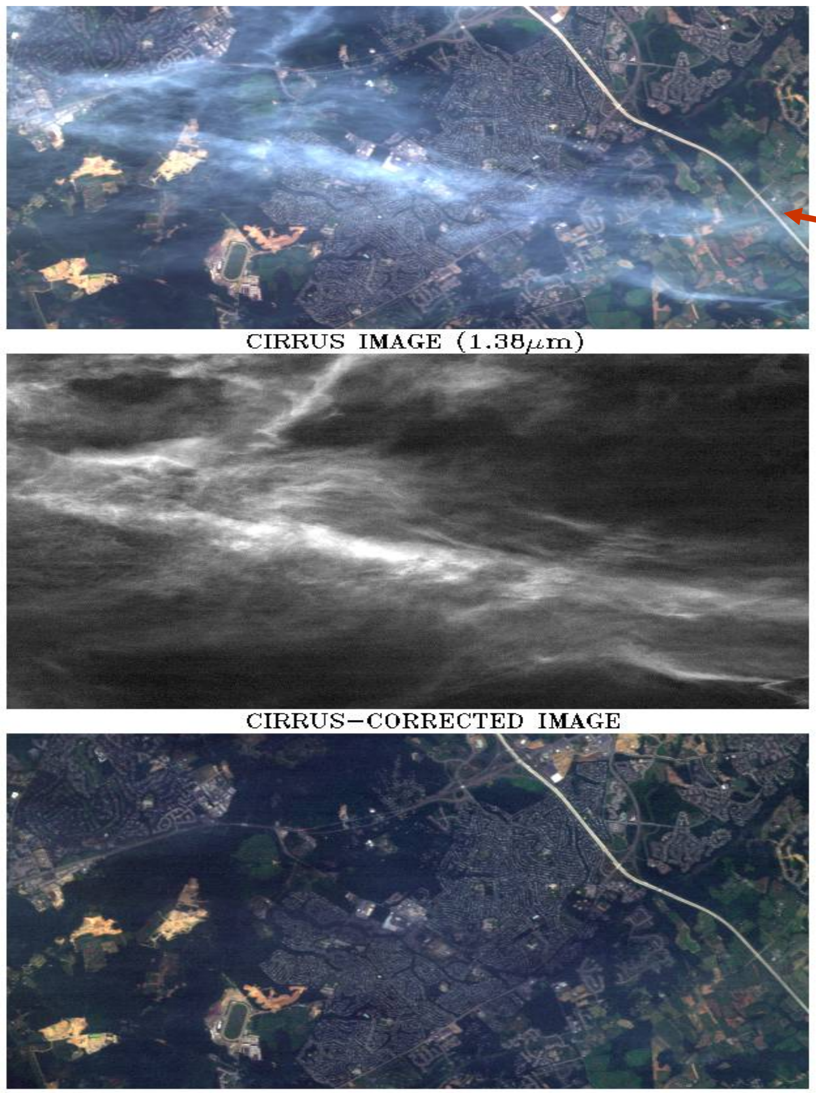

AVIRIS Image, 9/4/1992, Monterey, CA (R:0.65, G:.86, B:.47)

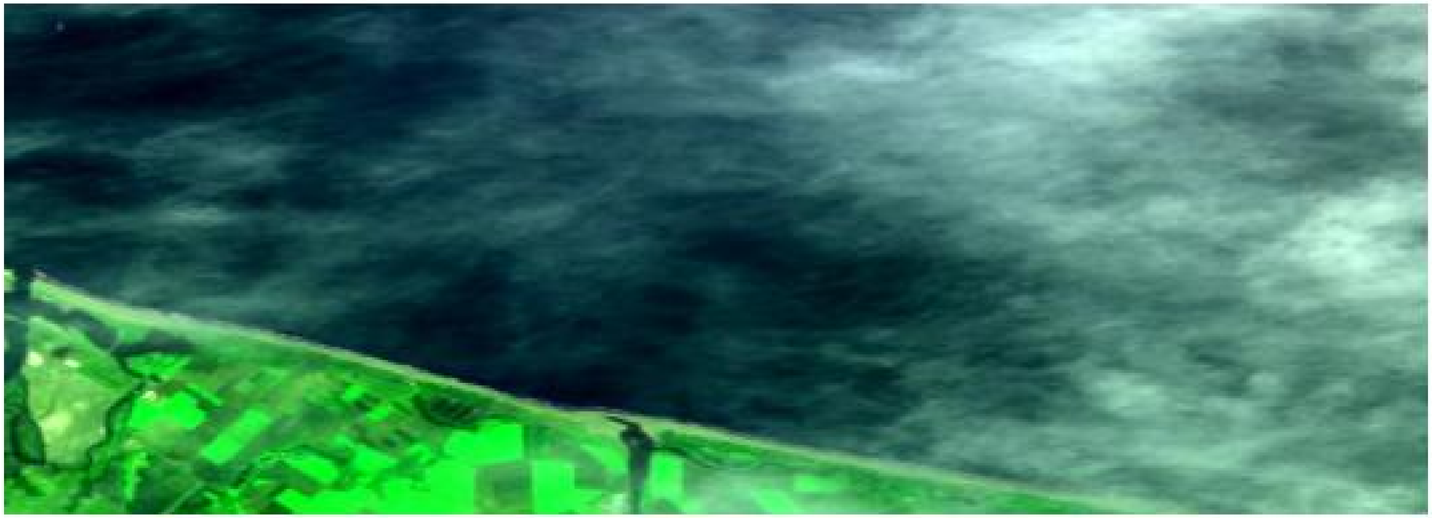

1.38 VS 0.65

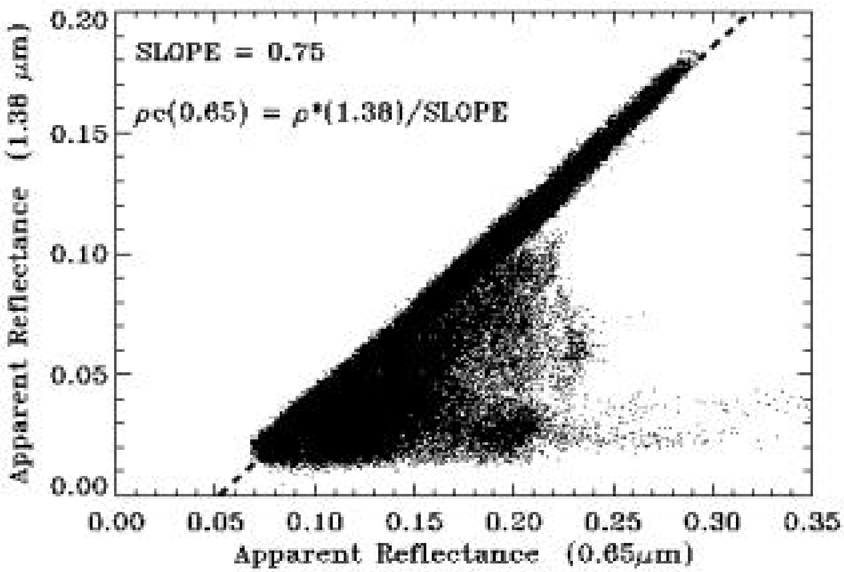

1.38 VS 1.64

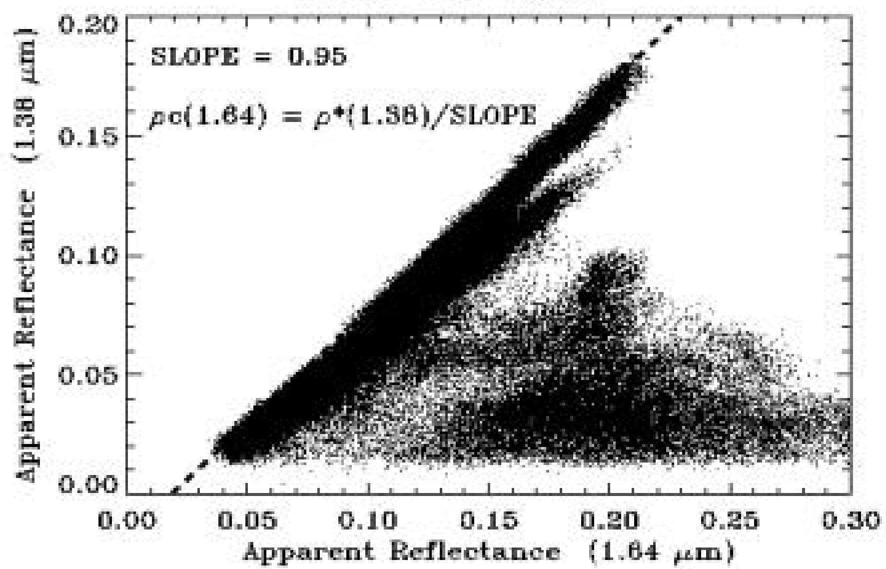

EQUATIONS

The apparent reflectance at the satellite level is defined as:

$$\rho\lambda^* = \pi L c\lambda / (\mu_0 E_{0})$$

$$\rho\lambda^* = \rho c\lambda + T c\lambda \, \rho\lambda / (1 - S c\lambda \, \rho\lambda) \qquad (1)$$

$\rho c\lambda$: path radiance due to cirrus;

$S c\lambda$: cloud scattering of upward radiation back to surface;

$\rho\lambda$: Surface reflectance;

If $S c\lambda << 1$, Eq. (1) becomes: $\rho\lambda^* = \rho c\lambda + T c\lambda \, \rho\lambda$ (2)

We found an empirical relation: $\rho c\lambda = \rho c1.375 / K_a$, (3)

where K_a is derived from a scatter plot.

Substituting Eq. (3) into (2), we get

$$T c\lambda \, \rho\lambda = \rho\lambda^* - \rho c1.375 / K_a \qquad (4)$$

To a good approximation: $T c\lambda = 1 - \rho c\lambda$,

& $\rho\lambda = [\rho\lambda^* - \rho c1.375 / K_a] / (1 - \rho c1.375 / K_a)$ (5)

Cirrus Removal For AVIRIS 0.65-μm Channel

0.65 μm Image
(Un-corrected)

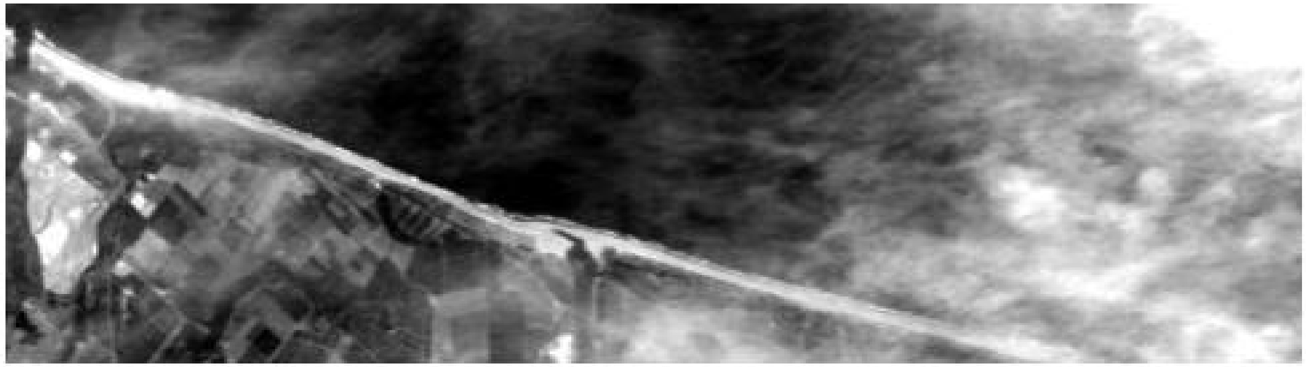

1.38 μm Image

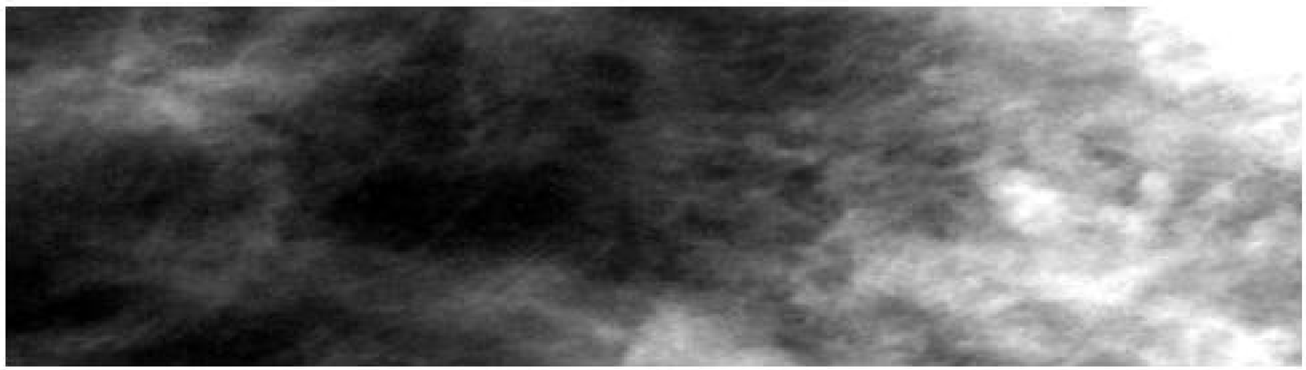

0.65 μm Image
(Cirrus-Corrected)

Cirrus Removal For AVIRIS 1.64-μm Channel

1.64 μm Image
(Un-corrected)

1.38 μm Image

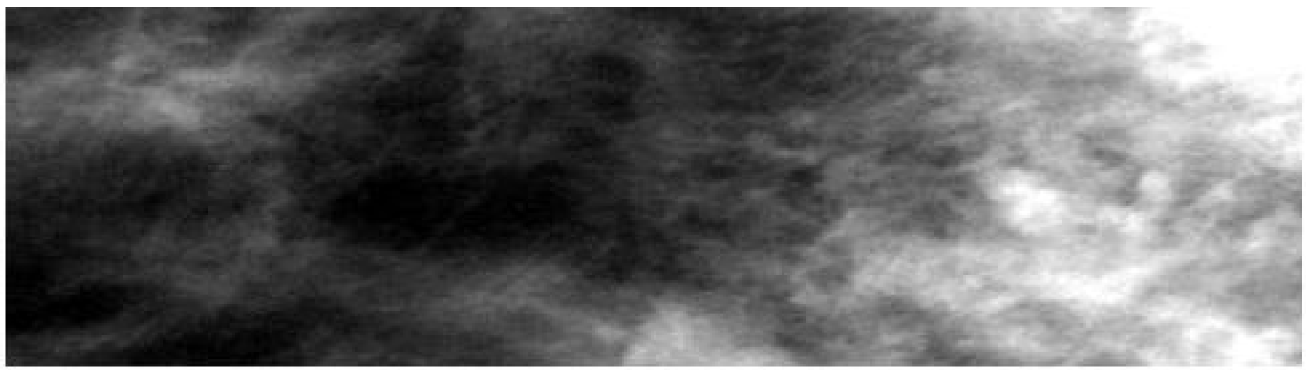

1.64 μm Image
(Cirrus-Corrected)

A pair of AVIRIS images acquired over Gainsville, Florida – with more cirrus (2nd pass) & less cirrus (3rd pass)

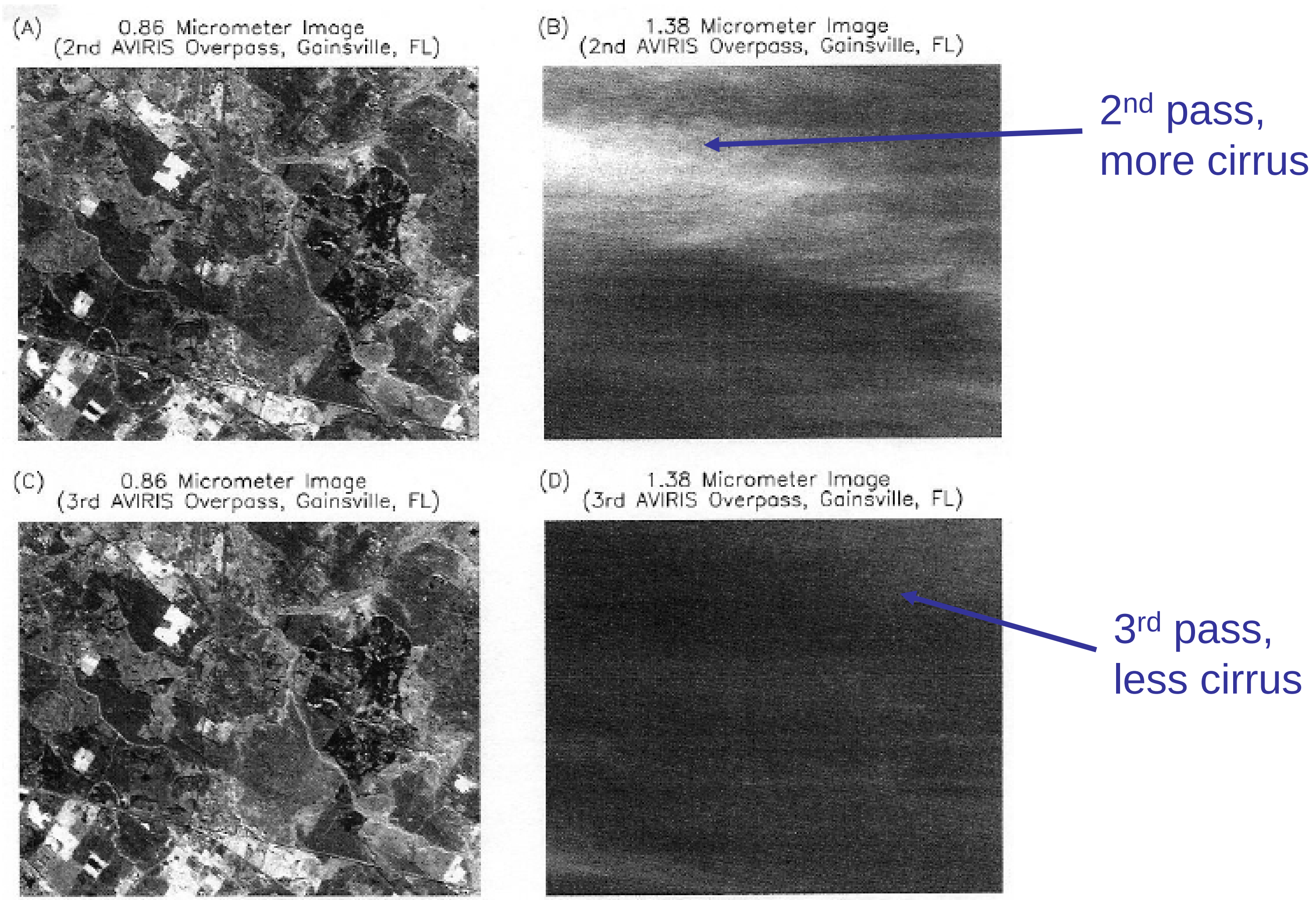

Un-corrected and Cirrus-corrected NDVI Images

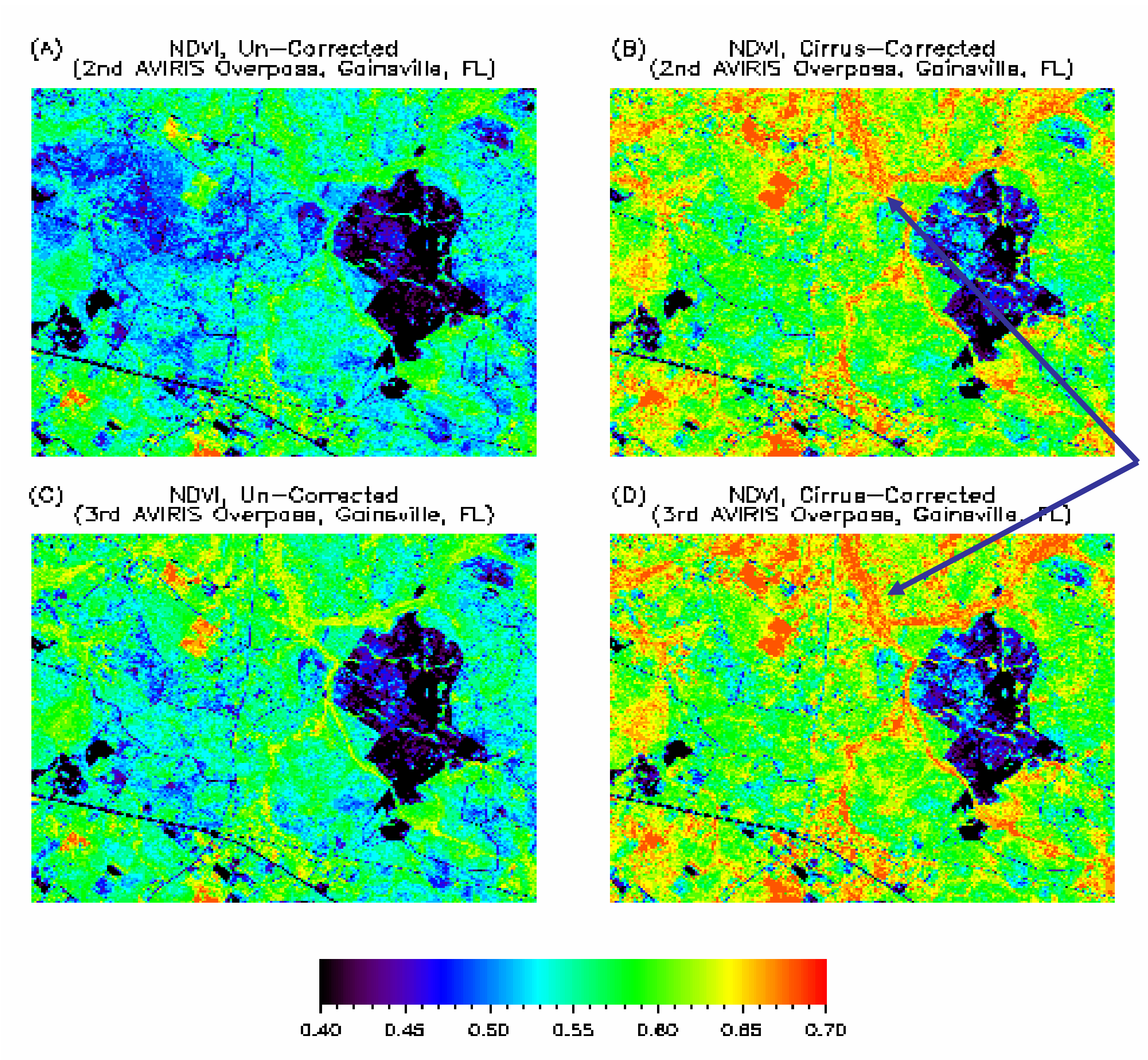

After cirrus correction, the two NDVI images appear identical.

Histograms for the Un-corrected and Cirrus-corrected NDVI Images

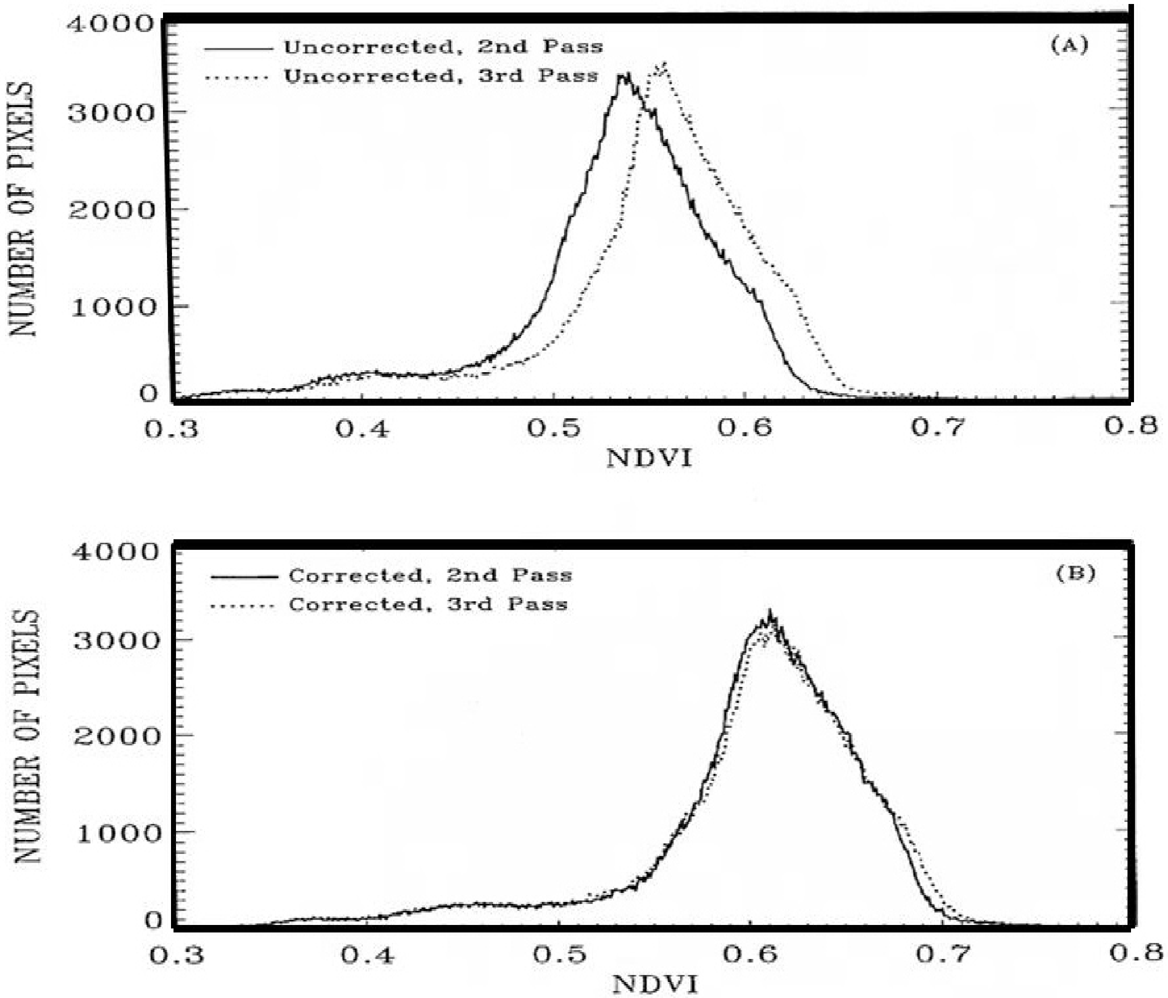

Un-corrected

Cirrus-corrected

Figure 7. (A) Histograms of uncorrected NDVI images obtained from the second and the third pass AVIRIS data sets over Gainesville, Florida. (B) Similar to (A), except for cirrus-corrected NDVI images.

Part IV: Spectrum-matching techniques for hyperspectral data analysis

Wavelength Calibrations Using Atmospheric Bands

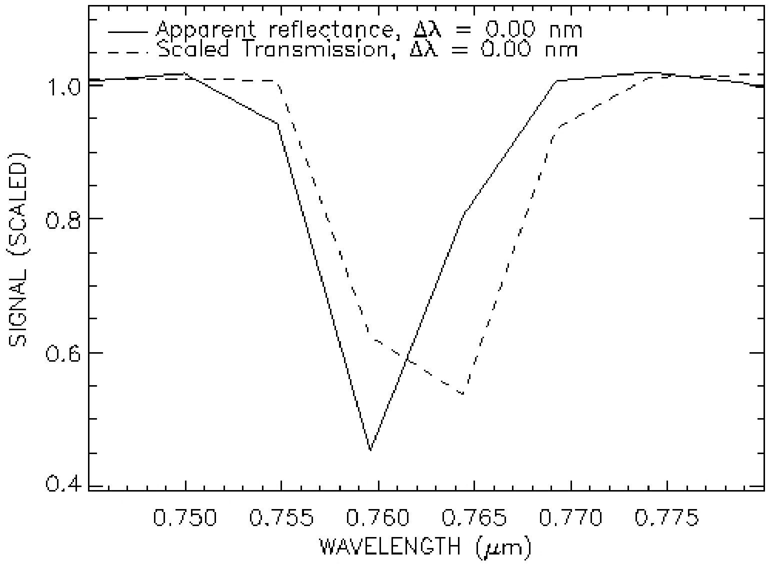

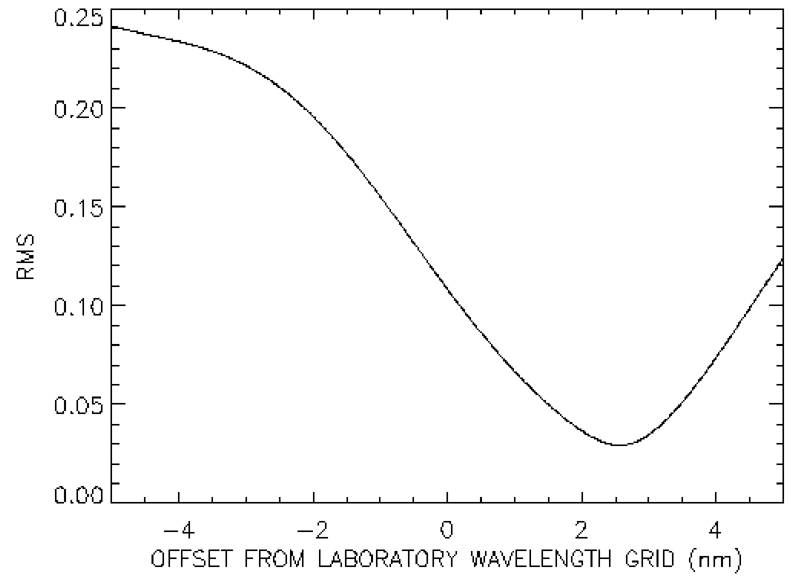

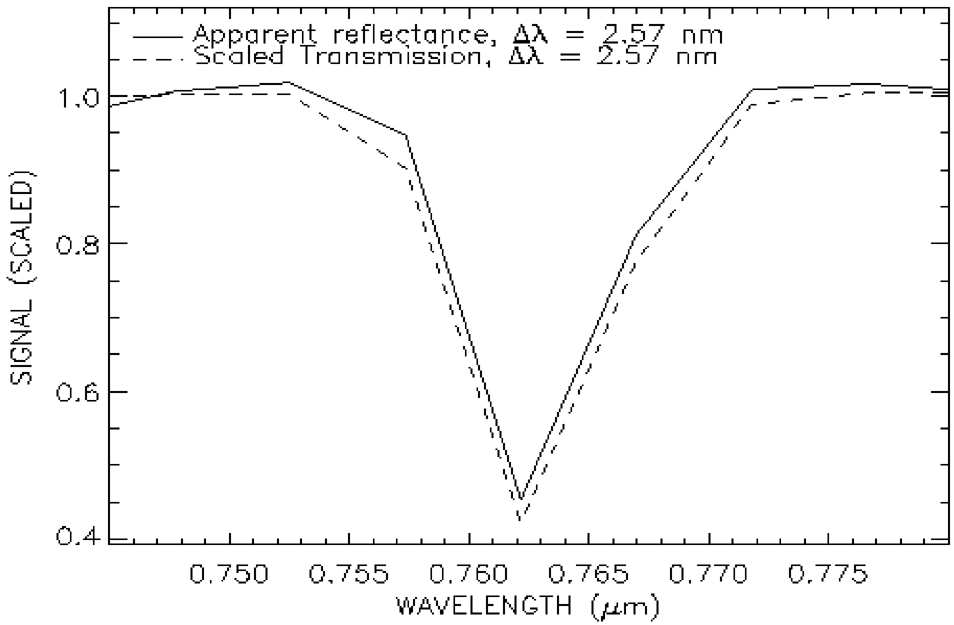

Spectral Resolution Estimates

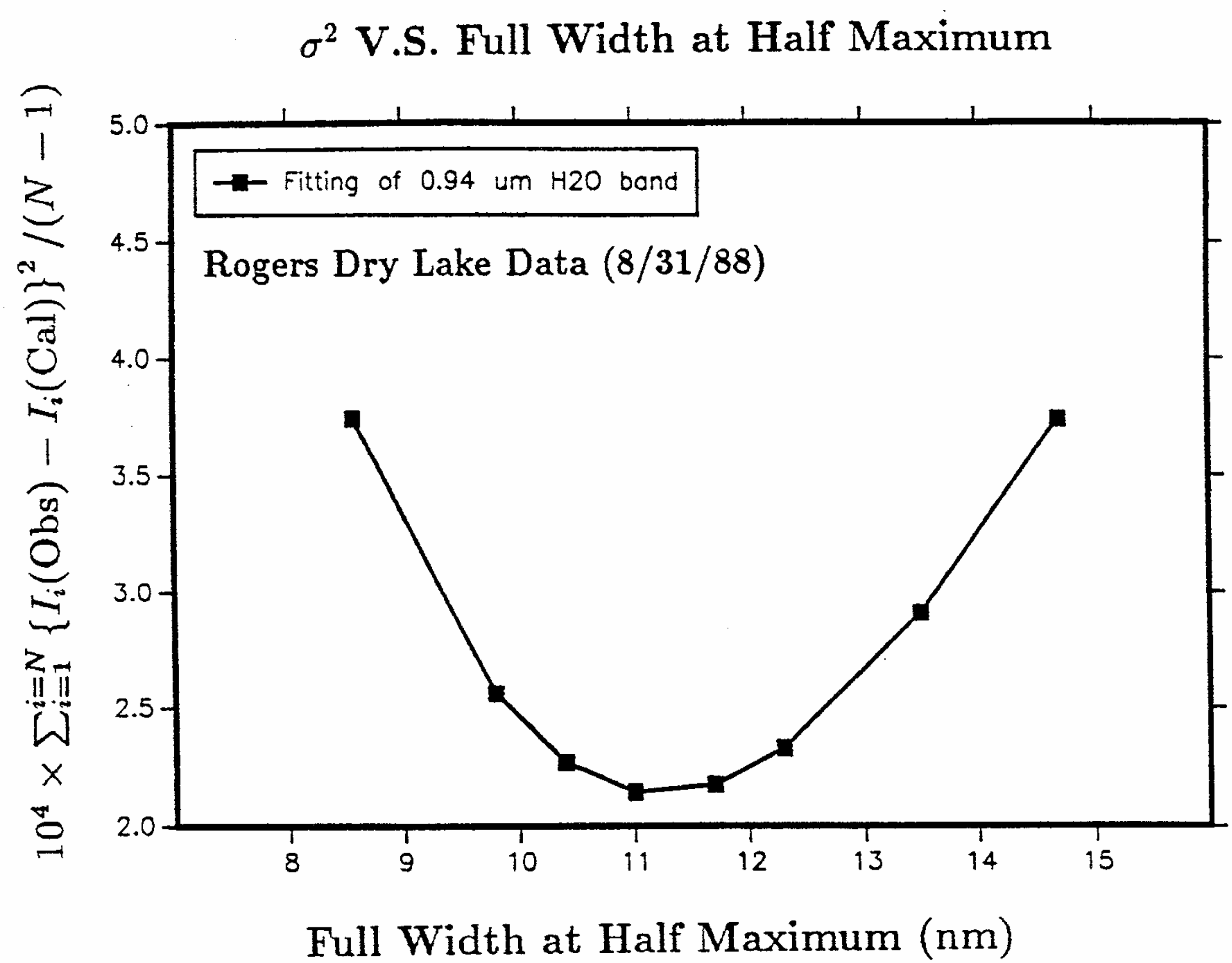

Spectrum-Matching for Simultaneous Retrieval of Atmospheric Water Vapor and Vegetation Liquid Water Content

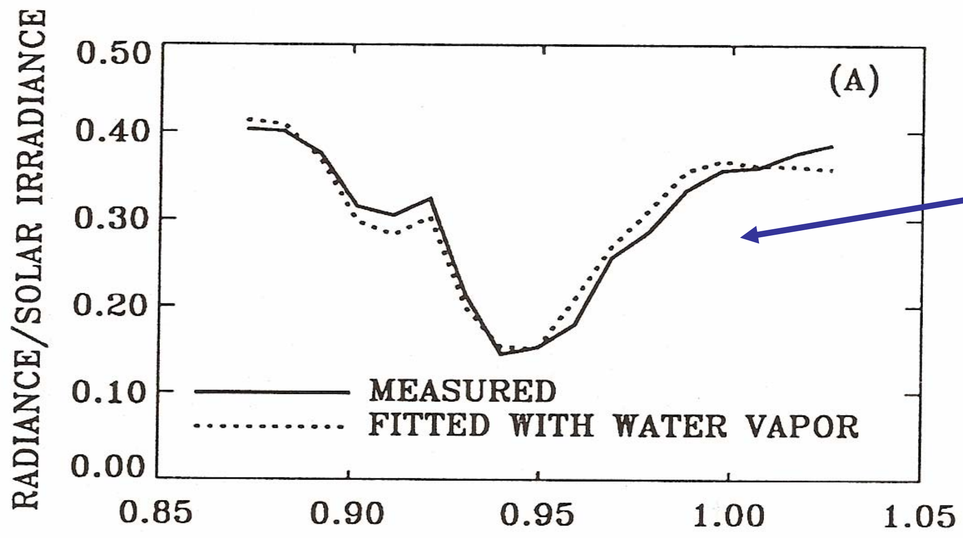

Matching of an AVIRIS spectrum over green vegetation with atmospheric water vapor spectrum alone – not good match

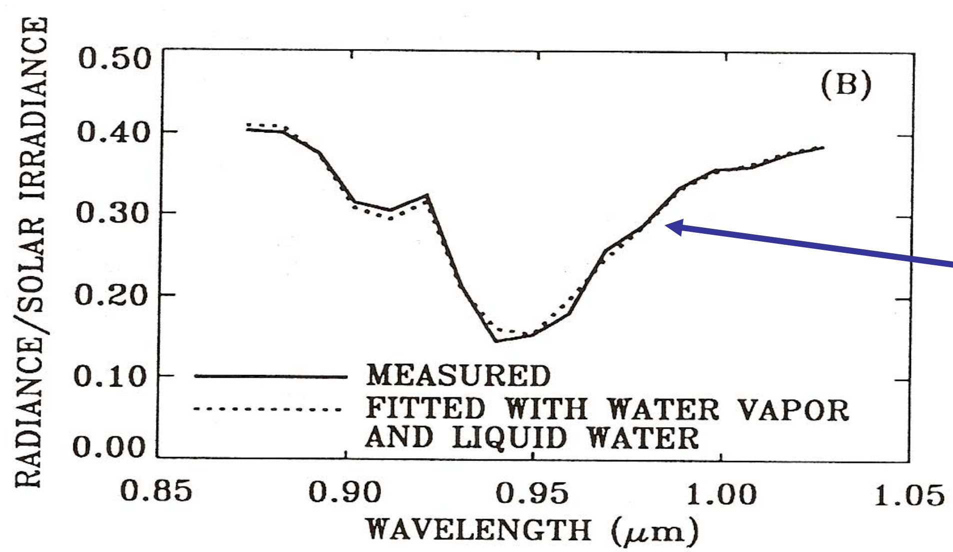

The matching result is improved significantly after the inclusion of water vapor and liquid water spectra in the matching process.

Incorporation of UV channels (380 nm, 400 nm)

Japanese GLI Image with Asian Dusts

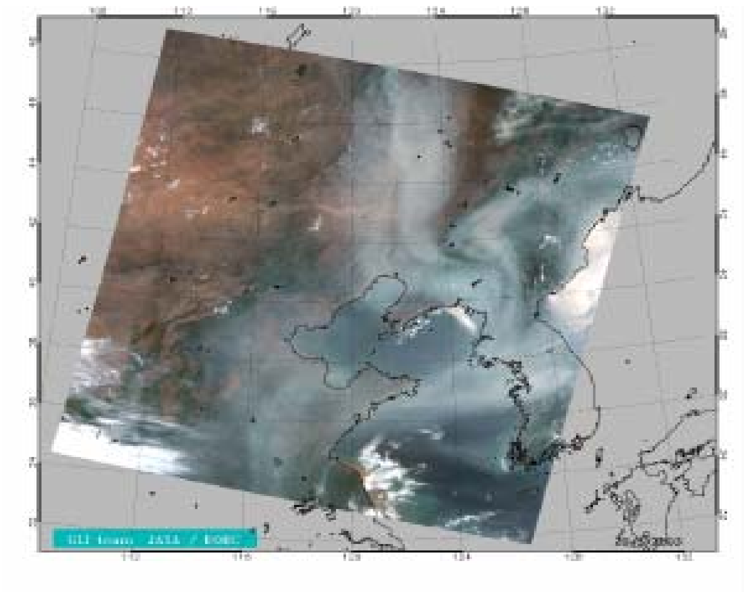

Ratio Image (400 nm/380 nm) Detected Dusts

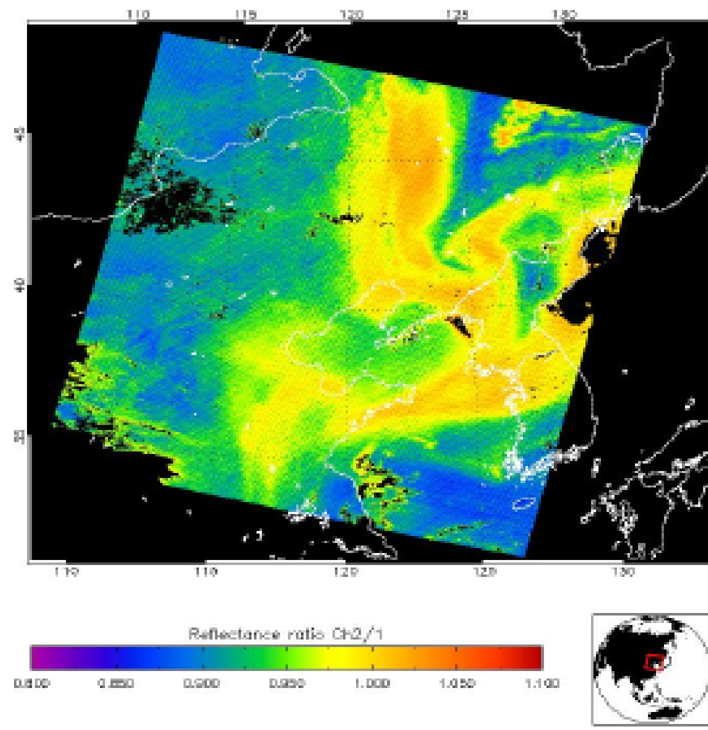

- The Japanese GLI ratio image of 400 nm/380 nm detected very nicely the Asian dusts over both land and water surfaces. Newer generation of imaging spectrometers have UV channels as short as 380 nm.
- Therefore, we need to add a module to derive aerosol models and optical depths using UV channels.